2017

Designing and Development of a Photobioreactor for Optimizing the Growth of Micro Algae and Studying Its Growth Parameters

Sarmila Katuwal
South Dakota State University

DESIGNING AND DEVELOPMENT OF A PHOTOBIOREACTOR FOR OPTIMIZING THE GROWTH OF MICRO ALGAE AND STUDYING ITS GROWTH PARAMETERS

BY

SARMILA KATUWAL

A thesis submitted in partial fulfillment of the requirements for the

Master of Science

Major in Agricultural and Biosystems Engineering

South Dakota State University

2017

DESIGNING AND DEVELOPMENT OF A PHOTOBIOREACTOR FOR OPTIMIZING THE GROWTH OF MICRO ALGAE AND STUDYING ITS GROWTH PARAMETERS

SARMILA KATUWAL

This thesis is approved as a creditable and independent investigation by a candidate for the Master of Science in Agricultural and Biosystems Engineering degree and is acceptable for meeting the thesis requirements for this degree. Acceptance of this thesis does not imply that the conclusions reached by the candidate are necessarily the conclusions of the major department.

Gary A. Anderson, Ph.D.
Major and Thesis Advisor Date

Van Kelley, Ph.D.
Head, Department of Agricultural and Biosystems Engineering Date

Dean, Graduate School Date

AKNOWLEDGEMENTS

It’s my great pleasure to thank you everyone who helped me during my research and course work at South Dakota State University. I would like to express my sincere gratitude to my research advisor Dr. Gary A. Anderson for his continuous support, guidance, and mentoring throughout my research work. I am very thankful for his valuable comments, suggestions, and encouragements in accomplishing this thesis.

I would like to thank my research committee members Dr. Zhengrong Gu, Dr. Eric Nelson, and Dr. Kommareddy for their unconditional support and valuable input in completing this research. I would like to thank Dr. Tylor Johnson for providing the culture of cyanobacteria and other lab support that helped me to conduct the experiment smoothly. I would like to thank Dr. Bishnu Karki for her technical assistance during lab work and handling lab instruments.

I would also like to thank to Scott Cortus for his continuous technical support to conduct lab work. I would like to thank faculties and non-faculties members Department of Agricultural Engineering who helped me during my stay in the department. I would also like to thank my colleagues Surya, Anand, and Utsav.

Finally, I would like to express my immeasurable appreciation to my parents and my husband Shailendra Singh. Without their unconditional love, support, and encouragement, none of this would be possible.

DISCLAIMER

The trade names were exclusively used to meet the thesis requirements for the Master's Degree at the South Dakota State University. Any reference in this thesis to specific commercial products, processes, or services by trade name, trademark, manufacturer, or otherwise, does not constitute or imply its endorsement, recommendation, or favoring by the South Dakota State University. The views and opinions of the author expressed herein do not state or reflect those of the South Dakota State University, and shall not be used for advertising or product endorsement purposes.

TABLE OF CONTENTS

ABBREVIATIONS

BOD	:	Biochemical Oxygen Demand
BTU	:	British Thermal Unit
DO	:	Dissolved Oxygen
EIA	:	Energy Information Administration
ENU	:	Extent Non-Uniformity
LED	:	Light Emitting Diodes
ORP	:	Oxidation Reduction Potential
PAR	:	Photosynthetic Active Radiation
PBR	:	Photobioreator
PC	:	Poly Carbonate
PE	:	Polyethene
PMMA:		Poly Methyl Methacrylate
PVC	:	Polyvinyl Chloride
SVR	:	Surface to Volume Ratio
TAG	:	Triacylglycerol

LIST OF FIGURES

LIST OF TABLES

ABSTRACT

DESIGNING AND DEVELOPMENT OF A PHOTOBIOREACTOR FOR OPTIMIZING THE GROWTH OF MICRO ALGAE AND STUDYING ITS GROWTH PARAMETERS

SARMILA KATUWAL

2017

This thesis presents the estimated value of materials required to grow 1g of biomass and the analysis of the light intensity with respect to flow path and flow rate. This thesis aims to design the sparger for a flat plate Photobioreactor, study the flow patterns at different flow rate of air flow and check the performance of flat plate PBR by growing the cyanobacteria.

The estimated value to produce 1g of biomass ($C_{44.6}H_7O_{25}N_{7.68}P_{0.9}S_{0.3}$) was 0.099g of N, 0.493g of C, 0.160 g of Na, 0.026 g of P, 0.009 g of S, and 0.007 g of Mg. The energy required to fix carbon atoms in 1 mole of biomass was found to be 78,584,302 J. The net energy loss of the system was calculated by subtracting net enthalpy of reactants from net enthalpy of product which was found to be -3800.724 KJ.

Light plays a great role in the performance of PBR. The equation was also developed to find the relationship of light intensity with path length and gas flow rate. The sparger plays a major role in deciding the performance of the PBR. It is one of the means for mixing so that the gas can pass though the growth medium by bubble which is created by the passing the gas through the holes of the sparger. Mixing helps in proper distribution of nutrients to the medium in Photobioreactor (PBR), maintaining the uniform

temperature. The sparger was designed using a SPARGER software built on a Java platform to simulate the flow and pressure distribution along its length. Sparger diameter of 0.5 inch was designed with a hole diameter of 1/32 inch and spacing of 4.04 cm. The simulation result showed non-uniformity of less than 5% and the percentage of air-remaining after the last hole less than 1%.

With the designed sparger the flow patterns of bubbles were observed in 160L water in three different conditions. The first one was using the different number of sparger pipes ranging from 1 to 4. The second one is using the different gas flow rate and the third one is observing the flow patterns at different height. Larger number of sparger pipes shows the better mixing, 10LPM flow rate was observed to have a uniform bubble distribution and at the higher depth the flow was observed to be air lift.

The designed sparger for the PBR system was used in a PBR to grow cyanobacteria. Cyanobacteria was grown on BG-11 media and the highest concentration of biomass was found on 13th day with a value of 928 mg/L. The physical parameters like Oxidation Reduction Potential (ORP), Dissolved Oxygen (DO), pH and temperature were studied. The range of ORP, DO, pH and temperature were found to be 169.76 to 327.67 mV, 8.68 to 8.20 mg/L, 6.15 to 8.09 and, 26.81°C to 30.91°C respectively. The observed results were compared to the small reactor results.

Keywords: Photobioreactor, Sparger, Cyanobacteria, flowrate, ORP, pH, DO, and Temperature

1. INTRODUCTION

1.1. Energy consumption pattern around the globe

The world energy consumption in 2012 was found to be 549 quadrillion BTUs and is expected to reach 815 quadrillion BTU in 2040 which means that the world is demanding an extra 265 quadrillion BTU energy within next 28 years (Martin, 2013). The sources of energy on which world is dependent on include coal, oil, gas, hydro, nuclear, biomass, and solar energy. About 79% of the energy consumed is from fossil fuels which accounts for 30% of oil, 27 % of coal, and 22% of natural gas around the globe as illustrated in Figure 1. This energy consumption pattern indicates that the primary energy sources used worldwide is highly dependent on non-renewable energy sources.

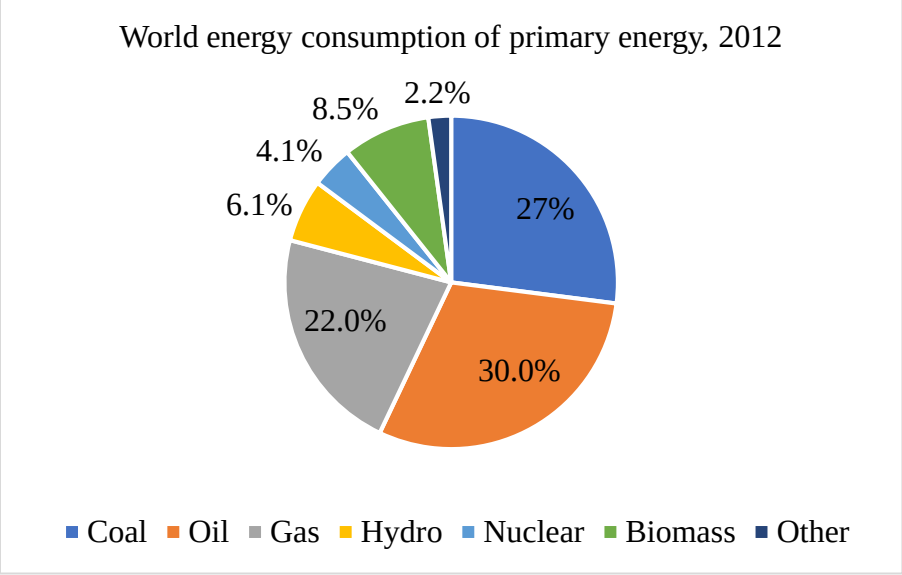

Figure 1. World energy consumption 2012 (Finley, 2013)

The energy generated from these non-renewable sources are used everywhere including transportation, residential, industrial, electric power, and commercial areas. With the

current energy consumption pattern and energy demand, it is undeniable that non-renewable energy sources will be depleted one day. This massive dependency on non-renewable energy sources and the risk of future depletion of such sources might invite an energy crisis around the globe. Thus, there is a pressing need to find alternative renewable energy sources that can be substituted for non-renewable energy sources.

1.2. Energy Demands and Importance of Renewable Energy

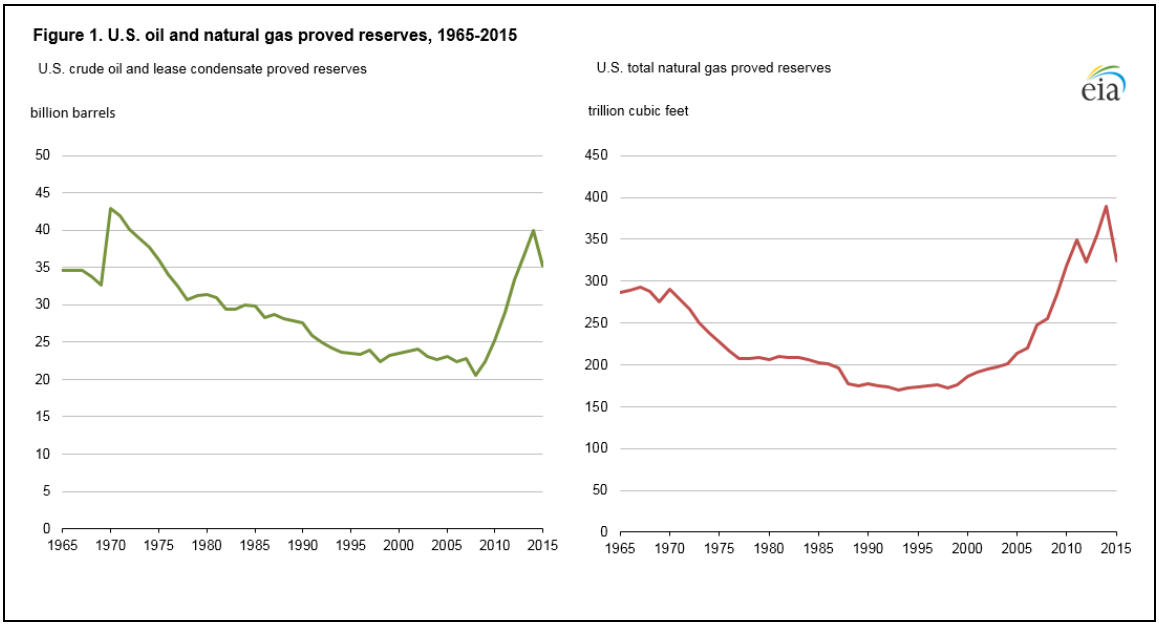

Figure 2. U.S. annual proved reserves crude oil and natural gas (EIA, 2015)

Figure 2 shows the U.S. reserve of crude oil and gas annually from 1964 to 2014. It is found that the reserve of crude oil and natural gas was in a decreasing trend from 1972 through 2012 and has started increasing from 2013 onwards. The increase in the reserve is due to the new drilling technology known as hydraulic fracturing or fracking (Fitzgerald, 2012).

Figure 3 shows the US primary energy consumption by source and sector for 2016 (EIA, 2017). The left side represents the share of the sources, and the right side represents the

demand sector indicating about 81% of energy usage is fossil fuel, natural gas, and coal. There is an increase in energy consumption from petroleum and natural gas of by 1% and 3% respectively and the coal consumption is decreased by 5% compared to the data of 2012 (Energy Information, 2012). This may be because of the fracking of oil in the U.S. Petroleum alone accounts for about 37% of the total energy. This portion of energy contributes about 71% to the transportation, 23% to industries, 5% to the residential and commercial sectors, and 1% in generating electric power. Considering energy demand fulfillment for the transportation industry, petroleum alone fulfills about 93% of the demand, and the rest is from natural gas and renewable energy. Similarly, contribution from the other sources to this sector are shown in the Figure 3.

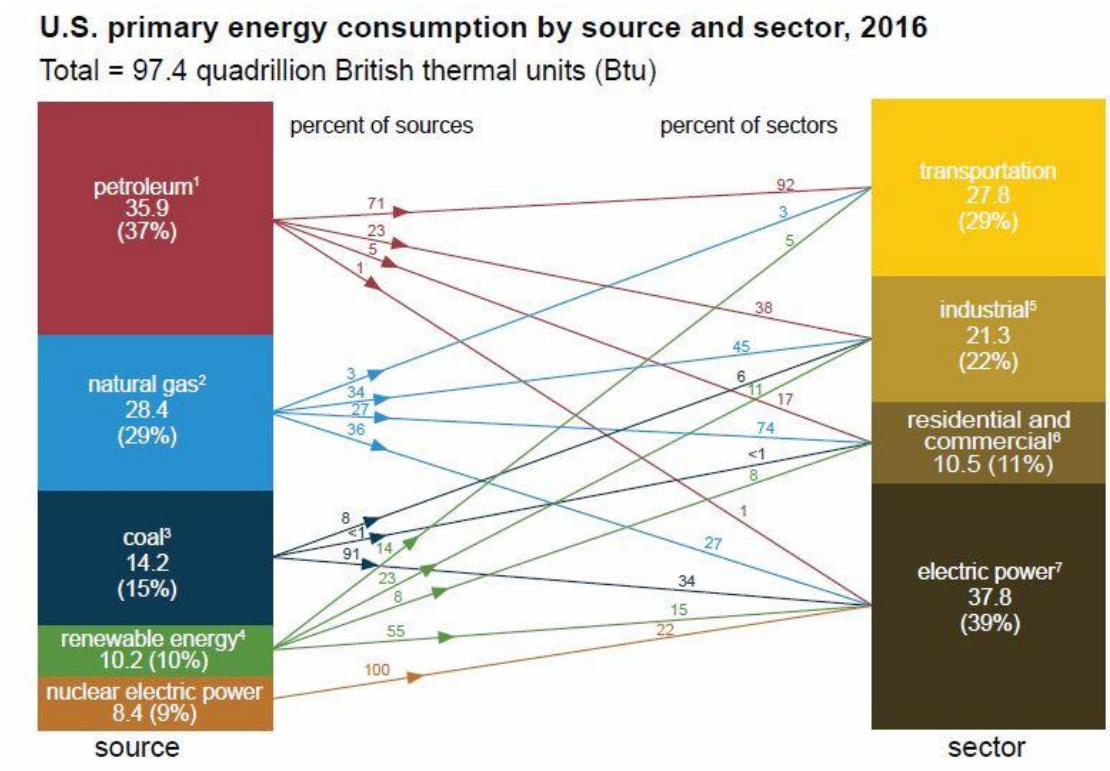

Figure 3. US primary energy consumption, 2016 by sources (EIA, 2017)

Consumption of non-renewable energy and its supply-demand is population driven. Over the past decades, the increasing population demand for these energy sources has increased substantially. This increased energy demand has imposed a greater risk to the environment resulting from the very high carbon footprint possessed by the use of fossil fuels. Research studies have shown that the current usage rate of fossil fuels is directly associated with climate change and greenhouse gas emission (Höök and Tang, 2013). At the current utilization rate, these sources will be at a risk of depletion as well as imposing a substantial threat to both energy and environment sustainability. Therefore, there is a dire need of developing cleaner technology.

1.3. Biomass energy and feedstock for biofuels

Biomass energy is a form of the renewable energy produced from trees, plants, forest residues, agricultural residues, energy crops, microalgae, animal wastes and waste materials. Among all the biomass energy, biofuel is the most dominate and is primarily consumed by transportation.

Cover crops are considered the most common biomass source for producing bioenergy. Studies suggest that it consumes CO_2 and produces fewer emissions compared to other biomass. On average, cover crops can yield around 2-3 tons/acre of biomass annually and can go up to 5 tons/acre if conditions are favorable (Kemp and Lyutse, 2011). Some of the energy crops that are commonly used worldwide for producing biofuels are corn, soybean, rapeseed, and sugarcane. In the United States, corn is used for producing ethanol whereas soybean is used for producing biodiesel. Likewise, rapeseed is commonly used for producing biodiesel in Europe whereas sugarcane is used for producing biodiesel and ethanol and its molasses for heating purpose in Brazil. Biofuels

extracted from these food crops in the form of oil, sugar, and starches are called first-generation biofuels and are also known as conventional biofuels (Luque et al., 2008). Although these crops are good source for producing biofuels, there are some disadvantages associated with them. One primary concern is food insecurity resulting from high consumption of food crops for producing biofuels (Brennan and Owende, 2010).

The next source used for producing bioenergy is non-edible feedstock like vegetable oils, fats and nonfood products (Luque et al., 2008). Biofuel generated from lignocellulose is called second-generation biofuel. Cellulosic biofuels produced from agricultural residue, grass, shrubs, flowers, and trees is considered to have no impact on food production and usually derived from primary producers with high energy content. According to the U.S. Environmental Protection Agency (EPA) and the California Air Resources Board, cellulosic biofuels have played a considerable role in the reduction of global warming emissions (Martin, 2010). The estimated total biomass available from crop residues is more than 3,000 PJ/year and is considered as the biggest source of biomass followed by switchgrass on CRP land.

According to research, biomass production globally is estimated to be 220 billion dry tons /year (Hislop and Hall, 1996). However, the United States alone has the biomass production potential of 368 million dry tons per year from forest land and 998 million dry tons per year from agricultural land which can contribute more than one-third of the current demand of transportation fuels (Perlack et al., 2005).

To meet biodiesel demand from renewable energy sources alternative feedstock should be explored. Research studies have shown that microalgae possess the potential to replace

the current demand for biodiesel. Biofuels generated from microalgae and cyanobacteria are known as third generation biofuels (Ahmad et al., 2011). The biofuel produced from the metabolic engineering of microalgae is called the fourth generation of biofuel (Lü et al., 2011). Both third and fourth generation of biofuels are generated from the microalgae biomass but the difference is the processing of microalgae verse product separation (Kagan, 2010). The disadvantages associated with this process are energy consumption for cultivation is high, problem of biomass contamination in open pond systems, problems of fouling and the high cost of cleaning, and photoinhibition (Dutta et al., 2014; Ruffing, 2011; Singh et al., 2011). Fourth generation of biofuel has the ability to capture more CO_2, provide a high yield of microalgae with high lipid content, and has a high production rate (Dutta et al., 2014).

Algae are classified into two groups: microalgae and macroalgae. Table 1 shows the differences between micro-algae and macro-algae.

Table 1. Difference between micro and macro algae

Microalgae	Macroalgae
High oil yield content	Low lipid and carbohydrate
Challenging inefficient cultivation and harvesting	Low-cost cultivation and harvesting
Potential for biofuel	Potential for biofuel

1.4. Microalgae and its requirement for growing

Microalgae is a photosynthetic microorganism that can be converted into biomass in the presence of light and carbon dioxide. It follows the basic rule of photosynthesis as expressed by Davis et al (Davis et al., 2011):

CO_2+Nutrients+Light = O_2+Biomass

Microalgae are a unicellular species which exists individually or in chains or groups. Its size ranges from 1-30 μm and its negative charge ranges from -7 to -45 mV with a concentration of 0.5- 4 g/L. Nitrates, Phosphates, Iron, and trace elements are the major nutrients required for growing microalgae (Hundt and Reddy, 2011). It is suggested to blend CO_2 with air at a ratio of 0.2 to 5% to get the maximum growth (Kunjapur and Eldridge, 2010). The optimum temperature required is 20- 30°C (Chisti, 2013) and the pH should be in the range of 7-9 depending upon the species. The light absorption spectra is from 400-700 nm (PAR) (Berberoglu et al., 2007a).

1.5. Applications of Microalgae

Microalgae have been used for different purposes from ancient times. Because of its chemical composition, it has been used widely for various purposes like enhancing the nutritional value of food and animal feed, aquaculture, incorporated into cosmetics, etc. They are used in wastewater treatment for removing BOD, nutrients, heavy metals, pathogens, and heterotrophs, in biogas production, and toxicity monitoring (Munoz and Guieysse, 2006). Also, they are cultivated for a source of highly valuable molecules (Priyadarshani and Rath, 2012; Ting et al., 2017). Apart from these microalgae have the potential to be converted into biofuel. In recent years, many universities, companies, entrepreneurs, and organizations showed research interest on growing algae as it can be an alternate renewable feedstock for biodiesel production.

1.6. Why microalgae for biofuel?

High energy content

Micro-algae are composed of carbohydrates, proteins, fats and nucleic acids (Asmare et al., 2013). They contain higher concentration of biomass desired for large oil production for biofuel. The energy content of microalgae is 30 times higher than other crops used for biofuel production (Chisti, 2007).

Grows faster

Microalgae grows very quickly and can double every 24 hours (Chisti, 2007; Schneider, 2006). Studies suggest that it can be harvested in a short period of time and requires no seasonal waiting allowing continuous production of feedstock.

Table 2 shows the oil yield of different energy crops and microalgae. The oil yield data indicates that microalgae have the potential to produce about 341 to 795 times more biodiesel than corn and 9 to 23 times more than oil palm.

Table 2. Different sources of biodiesel and its oil yield (Chisti, 2007)

Crops	Oil yield (L/Ha)
Corn	172
Soybean	446
Canola	1190
Jatropha	1892
Coconut	2689
Oil palm	5950
Microalgae (70 % oil by weight in biomass)	136,900
Microalgae (30 % oil by weight in biomass)	58,700

Land Requirements

Algae can be grown in any unused land, ponds or inside a closed room. Research studies have suggested that microalgae have the potential to produce substantially higher energy per unit of land area than other high-energy crops, depending on its species and growth conditions (Singh and Gu, 2010).

Cleaner technology

The source of carbon for growing algae is carbon dioxide. Thus, flue gas coming from a power plant can be utilized as a CO_2 source (Demirbas and Demirbas, 2010). Beside this, algae can be produced using nutrients such as phosphorus and nitrogen coming from wastewater treatment plant (Singh and Gu, 2010). Moreover, no herbicides or pesticides are required for algal cultivation and growth. Atmospheric carbon fixation capacity of microalgae is 10 to 50 times better than terrestrial crops (Verawaty et al., 2017).

1.7. Microalgae Productions Systems

Microalgae production can be done in two ways; pond systems (Figure 4) and photobioreactor (PBR) systems. The open pond system is the conventional method where microalgae can be grown in an open pond (Jiménez et al., 2003). There are four major types of open pond systems currently in use; shallow big ponds, tanks, circular ponds, and raceway ponds (Borowitzka, 1999). The carbon source from the atmosphere is used and the light source is sunlight. The advantages of this system are that it's less expensive, ease of cleaning, low maintenance, low energy inputs, and non-agricultural lands can be used (Chisti, 2008). Mixing is mostly done with a paddle wheel. The main limitations of this type of system are poor biomass productivity, contamination, limited algae strains,

and a large land requirement (Brennan and Owende, 2010). Since it is environment dependent, the biomass gets thick and light cannot penetrate deep into the system causing limited algae growth. Also, because it is an open system, evaporation losses are usually high.

The second one is the closed system also known as the photobioreactor (PBR) system. It was introduced to overcome the disadvantages of open pond system. This system mainly includes components of a photobioreactor, reactor volume, light, gas flow, and a sparger for mixing. A PBR is a vessel can be open, closed, or semi-closed and is made of transparent and waterproof materials in which microalgae cultivation is carried out (Ting et al., 2017).

Figure 4. Open pond system

Light plays a major role in making a PBR system effective and efficient. The amount of light that enters the PBR system impacts the growth rate of the micro-algae. Microalgae require plenty of photons to survive, and as the microalgae concentration increases, the

light penetration starts declining. The cells closer to the light source receive more light whereas the cells at the farthest point from the light source receive less light and this shade formation process is known as mutual shading (Pruvost et al., 2002).

Mixing is one of the factors that significantly affect the scaling of a PBR system. Mixing is principally done to keep the microalgae cells in suspension. The purpose of mixing is to maintain the uniform temperature, avoid settling of cells, and supply carbon dioxide to the medium while removing oxygen from the medium by increasing the mass transfer rate (Carvalho et al., 2006). Mixing depends on the types of devices used and the PBR selected. Gas flowrate and sparger design are two essential parameters for mixing and are interrelated.

A PBR system is said to be well designed if cells move periodically across the light gradient through a small pressure difference and a low shear rate. The other important aspect of a well-designed PBR system is reduced micro eddy formation resulting from mixing. Micro eddies form with a diameter less than 50 μm if the liquid velocity is greater than 1m/s. These micro eddies will damage cells, and therefore, it is suggested to have a mixing velocity of 20-50 cm/s to avoid micro eddy formation in the PBR system (Posten, 2009).

1.8. Project Significance

Considering the tremendous benefits of a PBR system, development and modification of PBRs by different researchers is underway. Besides the many advantages of a PBR system over traditional microalgae cultivation systems, it has some disadvantages too which are mostly associated with the initial investment. The cost of design and

development of a PBR system is considerably higher, and therefore, it still requires a substantial amount of research and testing to reduce the cost associated with it. As of now, no optimum photobioreactor has been developed since it is governed by many factors and design considerations (Socher et al., 2016). Also, several studies have been conducted on small-scale PBR systems, but very limited research has been done towards upgrading small-scale PBRs to large scale.

Design considerations of a PBR include selection of microalgae and mass & energy balances for light design and an understanding of mixing. Photo-inhibition (when the light intensity is very high) and photo- saturation (when the intensity is too low) are two other limiting factors for light penetration. Cells at the center of the PBR will not be exposed to light when the concentration gets thick and therefore limits the growth. To overcome this either the light path should be decreased or proper mixing should be done. Therefore, this research aims to study the relationships between light path length, and air flow rate. Also, uniform distribution of gas throughout a sparger is one of the problems encountered when designing a PBR. This work explores the design and scale up gas flow rate by designing the sparger to provide uniform distribution of air throughout a sparger.

Furthermore, the flow patterns are not consistent between smaller and bigger PBRs. Therefore, this research aims to study flow patterns for a bigger reactor and see if flow patterns are similar to a smaller one. The design of a PBR at large scale has been studied for growing microalgae used in biofuel production.

1.9. Objectives

The overall objective of this research was to scale up a PBR and optimize the growth of microalgae. The specific objectives are listed as below:

- To study the relations of light and path length and flow rate.
- To find the theoretical estimation of the materials balance and energy balance.
- To design an efficient sparger for growing microalgae using SPARGER software.
- Study the flow patterns and behavior of the flow in a 160L reactor.
- To run the photobioreactor to find the concentration of biomass produced and relate the concentration to the physical growth parameters.

2. LITERATURE REVIEW

2.1. Algae species and nutrient source

2.1.1. Microalgae species and its compositions

Thousands of microalgae and cyanobacteria species have been discovered on this planet. Microalgae species selection depends upon its application. For example six species (Chlorella vulgaris, Spirulina platensis, Nannochloropsis gaditana, Nannochloropsis oculata, Phaeodactylum tricornutum, and Porphyridium cruentum) of microalgae were tested (100 g) to analyze the biochemical composition for food application. The composition was found as 40 g protein, 18 g of carbohydrates, 12 g of fiber and 10 g of lipid on average (Matos et al., 2016). The composition of individual species is provided in Table 3.

Table 3. Chemical composition of species of microalgal biomass (Matos et al., 2016)

Species	Protein (%)	Carbohydrate (%)	Fiber (%)	Lipid (%)
Chlorella vulgaris	41.4	26.7	5.6	12.8
Spirulina platensis	42.8	21.5	8.5	5.5
Nannochloropsis gaditana	41.6	18.6	14.1	8.1
Nannochloropsis oculata	42.1	16.7	13.0	15.6
Phaeodactylum tricornutum	39	15.4	13.2	14.9
Porphyridium cruentum	35.4	12.5	18.3	5.3

Also, many research studies are focused on the selection of a microalgal species for biofuel production. For commercial biofuel production, research suggests to select a microalgae strain with high oil yield and fast-growth (Del Río et al., 2015).

Table 4. Different microalgae and cyanobacteria species and its lipid content (Sharathchandra and Rajashekhar, 2011; Zhan et al., 2016)

Microalgae species	Lipid content (%)
Chlorella sp. HQ	31.8±43.19
Chlorella ellipsoidea	16.85±7.85
Chlorella pyrenoidesa	18.02±5.36
Chlorella vulgaris	28.65±14.08
Scenedesmus dimorphus	30.59±1.25
Scenedesmus quadricauda	66.05±8.55
Scenedesmus obliquus	17.03±0.88
Scenedesmus sp. LX1	12.75±4.36
Oscillatoria calcuttensis	25.70±0.14
Oscillatoria acuminata	24.65±0.21
Nostoc linckia	18.45±0.07
Calothrix fusca	22.60±0.28
Lyngbya limnetica	18.10±0.14
Phormidium purpurescens	26.45±0.21
Microcystis aeruginosa	28.15±0.21
Lyngbya dendrobia	10.55±0.07
Oscillatoria perornata	14.10±0.14
Phormidium ambiguum	10.48±0.10
Oscillatoria amoena	18.63±0.18
Scytonema bohnerii	22.22±0.32
Oscillatoria chlorina	16.62±0.16

The composition of glycerol molecules bound to three fatty acids, Triacylglycerol (TAG) is the most common lipid available in microalgae (Abdo et al., 2014). The average lipid

content varies from 1% to 70% and can reach up to 90% for some species under certain conditions (Mata et al., 2010). The lipid content of commonly produced microalgae and cyanobacteria species are presented in Table 4.

2.1.2. Nutrients composition and source

There is no single formula for the nutrient calculation that can be applied to all the species. However, all the species have a minimum, optimum, and maximum nutrient requirements (Grobbelaar, 2010). Elemental mass balance is one approach used to estimate the minimum demand of the medium composition (Morweiser et al., 2010). In this method, the microalgae strain is selected first based on the need and depend upon its biomass composition. After selection of the microalgae strain, major ionic components are determined for calculating the nutrient requirement.

Also, the nutrient requirement depends upon sources that are used to cultivate the microalgae. Nitrate, Ammonia, and Urea are the sources of nitrogen whereas CO_2, HCO_3^- and organic carbon like acetate or glucose are the sources of Carbon (Cañedo and Lizárraga, 2016). If microalgae is cultivated in a PBR system with fresh water as a medium then artificial nutrients are prepared in the lab. Nutrient preparation in the lab is costly and therefore, to reduce feed cost, it is necessary to identify free and reliable sources of nutrients for microalgae production.

The one source that has potential to support the growth of microalgae is wastewater coming out from wastewater treatment plants. Such wastewater contains essential nutrients like N and P that have a vital role in microalgae growth (Verawaty et al., 2017). Since both N and P are pollutants. Growing microalgae using these nutrients will be

beneficial to both the environment and cost of microalgae production. It is reported that microalgae species like Scenedesmus sp, Chlorella sp, Scenedesmus sp, Phormidium sp, Botryococcus sp, Chlamydomonas sp and Spirulina sp have been used widely in wastewater treatment plants (Olguí, 2003). The other potential free nutrient source that can be used for microalgae production is flue gas coming from industry. Flue gas from industry is very toxic and harmful to the atmosphere and ozone layer (Brar et al., 2017). However, these gases contain nutrients required by microalgae for their growth. Thus, utilizing flue gases in microalgal production will help to reduce production cost and reduce environmental pollution resulting from harmful combustion gases.

2.2. Types of Photobioreactor (PBR) system

2.2.1. Tubular PBR

A tubular PBR is tubular in shape and is usually constructed of glass, PVC, or plastic and is the most common system used these days (Cañedo and Lizárraga, 2016). The attraction of this type of PBR is its simplicity and large illuminated surface area which is most appropriate for outdoor use (Figure 5). The diameter of the tube ranges from 10 mm to 60 mm (Posten, 2009) whereas the length varies from 10-100m (Xu, 2007). The diameter of the tube is kept small to increase light penetration in a reactor. For mass cultivation, the preferred liquid velocities are 0.2 m/s to 0.5 m/s (Morweiser et al., 2010). Mixing is normally done by a sparger forming bubbles (Singh and Sharma, 2012). A degasser unit is connected to the tubes to prevent high oxygen concentration from building up in the PBR system (Vree et al., 2015). Depending upon the tube orientation, it is referred to as horizontal, vertical, or inclined tubular PBR. The disadvantages are the accumulation of dissolved oxygen, excessive power consumption, high temperature, high pH, CO_2 and O_2

gradients, high capital and operating cost and photo limitations (Huang et al., 2017). Airlift and bubble columns are also tubular photobioreactors. This type of PBR works well under natural sunlight.

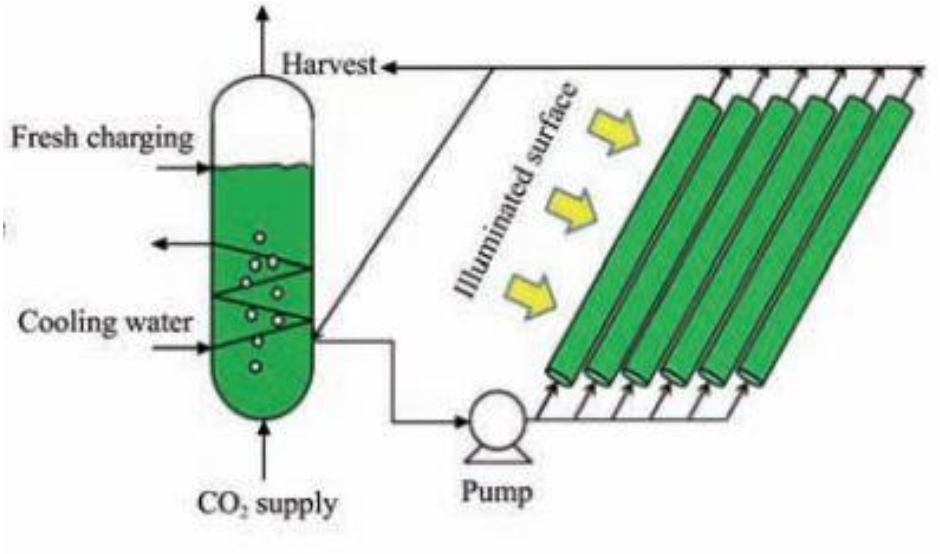

Figure 5. Horizontal tubular photobioreactor (Ting et al., 2017)

2.2.2. Bubble column PBR

In this PBR type, aeration occurs is the mixing process. The gas mixture is injected through the sparger forming bubbles which flow in an upward direction with no substantial upward or downward movement of medium flow (Figure 6). There is significant lateral movement of the medium so that the uniform distribution of nutrients and biomass concentration can be achieved (Anderson et al., 2014). The bubbles push the micro algae cells in a lateral direction. The primary need is that the height of the reactor is greater than twice the diameter (Singh and Sharma, 2012). It is used successfully in the medical industry. While designing, or scale up apart from light, the hydrodynamics of bubbles and flow regime should also be considered. The advantage of this type of PBR are surface area to volume ratio (SVR), heat and mass transfer in a satisfactory range, the

release of O_2 gas, good radial mixing is efficient, and fewer moving parts (Kumar et al., 2011).

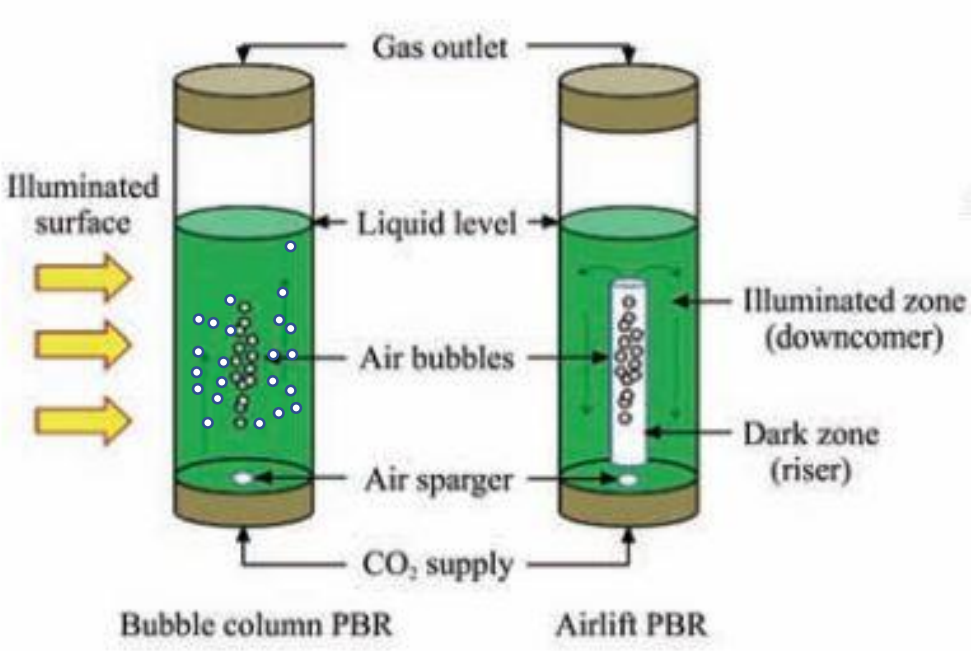

Figure 6. Bubble column and air lift photobioreactor (Ting et al., 2017)

2.2.3. Air lift PBR

An airlift PBR is different from a bubble column PBR because it has a riser and down comer (Figure 6). Riser function is similar to the bubble column method. Air and CO_2 are transferred to the riser through the sparger whereas as it is not sparged in the down comer (Kumar et al., 2011). The diameter of this reactor should not exceed 0.2 m, and the height should not be greater than 4m to prevent structural damage to the PBR and mutual shading (Wang et al., 2012). With the increase in the diameter of the tube, light penetration towards the center of the tube will be less. The materials used for this type of reactor are optically transparent material made up of glass and thermoplastics. These types of material do not have the strength to offer greater height and can be easily

damage by wind (Miron et al., 1999) .This type of reactor has the advantage of providing a flashing light effect in the PBR due to mixing. The bubbles transfer upward in the riser on the dark side and when they transfer to the down comer, then it is in the lit side of the PBR (Barbosa et al., 2003). Since mixing is the result of cyclical recirculation of bubbles, the PBR has a high mass transfer rate, low power consumption, and homogenous shear stress. It is one of the preferred methods for photobioreactors in industry (Huang et al., 2016). The important criteria while designing an air lift PBR is to increase the difference of gas holdup between the riser and down comer (Singh and Sharma, 2012). The disadvantages of this type of PBR are high capital cost and cleaning and maintenance (Soman and Shastri, 2015).

2.2.4. Flat plate PBR

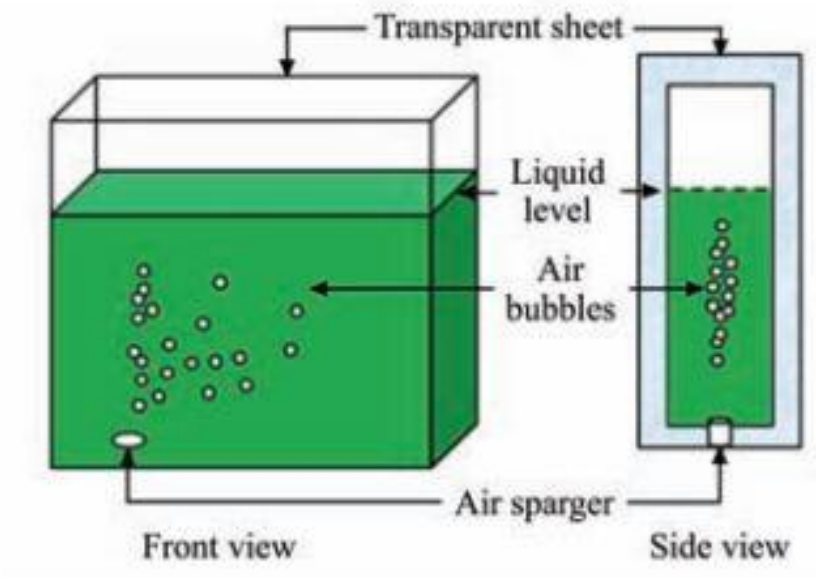

Figure 7. Front and side view of flat plate photobioreactor (Ting et al., 2017)

Flat plate PBRs are constructed using plastic or acrylic sheet. Mixing is either done by sparging or using a motor as shown in Figure 7 (Kumar et al., 2011). It is considered to have one of the high SVR compared to other PBR types. Surface to volume ratio in a PBR is the amount of the surface area illuminated by the light per unit the volume of the medium in the PBR system. Because of the large illuminated surface area, it has a low accumulation of dissolved oxygen, and high photosynthetic efficiency (Cañedo and Lizárraga, 2016). Mixing is commonly done by aeration or through a pump. There are ranges of dimensions for height and width, but the preferred one is lower than 1.5 m and 0.10 m wide respectively. A flat PBR can be inclined if illuminated by sunlight to reduce the light loss. The direction of the flat panels, angle and the number of panels per land unit are the factors affecting the biomass productivity in this type of PBR (Zijffers et al., 2008).The problems with this kind of PBR are fouling; cells attach to the plastic walls thus reducing light availability, and contamination.

2.2.5. Bag PBR

Micro algae are cultivated in the plastic bags in Bag PBRs (Figure 8). This system generally consists of plastics bags for growing microalgae, frame for supporting the structure and an aeration system to prevent the algal biomass from sedimentation (Ting et al., 2017). The design considerations for bag PBRs include size of the bag, selection and construction of materials, aeration method, and the structure for the frame. The advantage of this type of PBR is the low capital cost (Huang et al., 2017). Experiment with bag PBRs have been done from 5 L volume to 250 L volume for different species (Chen et al., 2013; Sierra et al., 2008).

Figure 8. Plastic bag photobioreactor (Huang et al., 2017)

Replacing the bag periodically is one of the major disadvantage of this type of PBR because disposing of the bag on large quantities has a negative impact on the environment (Wang et al., 2012). While photo limitation, bad mixing and leakage are the other disadvantages (Huang et al., 2017).

2.3. Design Consideration of Photobioreactor

Design of photobioreactors includes a number of factors that can influence the growth of cyanobacteria and algae in a PBR. The basic concept of PBR design is that it should have a proper source for carbon and energy (for example CO_2 and light) so that the photosynthesis process can take place efficiently. Apart from the carbon and light source, nutrients like carbohydrates, proteins, lipids, and nucleic acids are required, and proper mixing of these nutrients is an important aspect of PBR design.

2.3.1. Selection of materials

Almost every type of photobioreactor is constructed using transparent materials. The basic concept of proper transparent material selection is to provide the proper light

intensity inside the reactor (Wang et al., 2012). The materials usually employed for constructing the PBR are glass, polyethylene (PE), polycarbonate (PC), polyvinyl chloride (PVC), acrylic (Plexiglas, PMMA), silicate and fiberglass (Posten, 2012)**.** Also, selected materials should be toxic free, high strength, chemically stable, and easy to clean.

2.3.2. Physical and light properties of PBR

Table 5 and Table 6 show the physical and light characteristics of materials that are being used in PBR construction. Polythene has the highest light transmission, shear strength and lowest density indicating that it is lighter in weight for the same structural strength. Properties listed by polythene show that it should be one of the preferred PBR materials but its life span is less.

Table 5. Physical properties of PBR construction materials.

Materials	Energy Content (MJ/Kg)	Modulus of elasticity (psi)	Poisson's ratio	Material Density (Kg/m^3)	Melting point (°C)	Shear strength (psi)	Materials life span (yrs)	Tensile strength (psi)
Glass	25	9137377	0.20	2230	-	-	20	-
Polyvinyl chloride (PVC)	74	420000	0.410 @73°F	1400	60	-	-	7450
Polyethylene (PE),	78	530000	-	920	136	10500	3	6240
polycarbonate (PC)			-					
Plexiglas, PMMA	131	425000	-	1180	140	9000	20	9600
Fiber glass	11	-	-	-	-	-	-	-

Table 6. Optical properties of materials used for PBR

Materials	Light transmission (%)	Critical Angle	Refractive Index	Industry
Glass		43°	1.52 (1.473)	SCHOTT-tubular PBR
Polyvinyl chloride (PVC)	75		1.5	+GF +
Polyethylene (PE),	92 (1/8 inch)	46°	1.51	
Polycarbonate (PC)			1.60	
Plexiglas, PMMA	95	42.16°-45°	1.49	
Fiber glass	90	-	-	Solar Components Corporation

Glass has the lowest energy content which is preferred for a PBR. Glass PBRs are primarily used for hydrogen production from alga. Glass has the highest mass density which reflects that it is heavier and difficult to transport and handle (Burgess et al., 2007). Glass and polythene sleeves are mostly used for tubular photobioreactors. If chemical resistance is a concern then PVC is preferred. Acrylic sheet is an acceptable material for photobioreactors because transmission of light is high and reduced water evaporation loss when covered as it has low heat loss compared to glass. It has a long life span and a high melting point but the initial cost of the material is high. Good light transmission and least energy content are the reason for selecting this material. Fiber glass is a recent material that is being used for PBRs.

2.3.3. Methods of mixing

Mechanical mixers like paddles, mixers, and agitators are used for mixing. Magnetic stirring is used for small-scale PBRs whereas impeller methods are used for larger scale

PBRs, mostly in open pond PBRs. The paddle wheel is used must in PBRs. The diameter, impeller, and number of paddles on the wheel are the major parameters of the paddle wheel that should be accounted while designing the system to maintain uniform turbulence throughout the system. In general, achieving uniform turbulence throughout the system is a challenging part of PBR design. If the turbulence is low, settling may start and formation of the dead zones occurs. Three major flow regimes are considered; bubbly flow (homogenous), churn-turbulent flow (heterogeneous) and slug flow shown in Figure 9 (Vial et al., 2001).

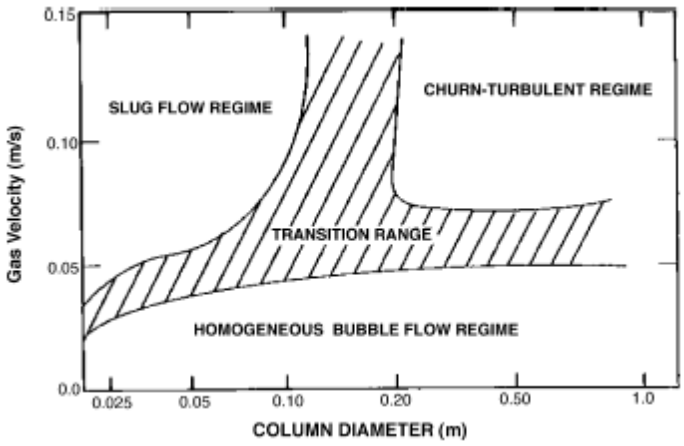

Figure 9. Flow regime of bubbles (Kantarci et al., 2005)

Superficial gas velocity (Ug) and hydraulic diameter play significant roles in categorizing the flow regimes. The homogeneous regime should have low superficial gas velocity and uniform bubble size and distribution. Heterogeneous flow is characterized by large bubbles and higher superficial gas velocities (Joshi et al., 2002; Veera and Joshi, 1999). Slug flow has been observed in small diameter laboratory columns at high gas flow rates (Hyndman et al., 1997). It is found that slug flow is observed in columns with diameters up to 15 cm (Miller, 1980). Many cyanobacterial strains are shear sensitive. However, the

exact shear rates associated with decreases in cell growth rates is unknown. While scaling-up, care should be taken that the flow is homogenous and the mixing is uniform so that cells get an equal amount of light thereby increasing the photosynthetic efficiency.

In the bubbling method, gas is injected through the sparger and when it comes in contact with liquid, bubble formation starts. It is one of the preferred methods for larger reactors. Type of sparger, geometry, gas velocities, and hydrodynamics of the bubbles play significant roles. These factors are very complex and interrelated to each other. The model developed for a small reactor may not predict the mixing in a larger PBR because a small change in PBR dimension will change the flow behavior (Prokop et al., 2015). Therefore, there is a problem in PBR scale up.

2.3.4. Sparger and its design considerations

A sparger consists of small orifices which help transfer the gas mixture into the microalgae growth medium through bubbles that reduce the oxygen content of the medium that is produced during the photosynthetic process (Singh and Sharma, 2012). The geometry of the spargers, diameter, spacing, size of the orifice, and number of the orifices are the important design aspects (Kulkarni and Joshi, 2011b). Inappropriate design of a sparger will lead to an inefficient photobioreactor system. Design considerations of the sparger include no weeping and to a lesser extent non-uniformity (ENU) (Kulkarni and Joshi, 2011a). A weeping condition occurs when the pressure of the gas injected into the sparger is less than the overall pressure of the growth medium. At this condition, instead of bubbling, the growth medium will enter inside the sparger through the holes. The factors that affect weeping are pressure drop along the sparger length, liquid height, the surface tension of the liquid. ENU is the indication of all the air

leaving the sparger along its length. It also tries to keep air flow rate through all the holes in the sparger the same. ENU occurs when the gas transfer along the length of sparger is not uniform and high non uniformity will lead to high pressure drop in the sparger and increase the chances of clogging the holes of sparger (Kulkarni et al., 2007). Therefore, if the sparger design is not appropriate, it may lead to weeping and the pressure drop might be increased so that the value of ENU will increase, leading to incomplete mixing in the PBR liquid. The amount of gas transferred to the photobioreactor plays a great role in developing the flow pattern. Bubble diameter and flow pattern play a substantial roles in designing the sparger and photobioreactor performance. Three types of bubbles are considered in sparger design. One is small bubbles which have a volume equivalent diameter less than 0.1 mm and are spherical in form. Another is intermediate bubbles which are ellipsoidal in shape. The last one are larger bubbles with diameters greater than 18 mm and are usually cap shaped with a volume greater than $3cm^3$ (Xue et al., 2008). Small diameter bubbles (micro meter) decrease the growth and productivity of algae because the size of the organism and the bubble size are similar and also has low light penetration. Also, microalgae and cyanobacteria which are trapped in the bubbles may get damaged when bubbles burst because of the energy released during the process (Camacho et al., 2001). If the bubble diameter is large, it can reduce the contact area between the air in the bubble and the medium thus reducing the mass transfer coefficient. The sparger should be selected in such a way that the bubble diameter ranges from 3mm - 7mm and the flow rate should be selected in such a way that microalgae are suspended while the superficial gas velocity that provides homogenous flow should be preferred for scale up. There are different types of spargers used commercially such as sieve plate,

radial, porous, spider, and ring type as shown Figure 10 and Figure 11 (Kulkarni et al., 2007).

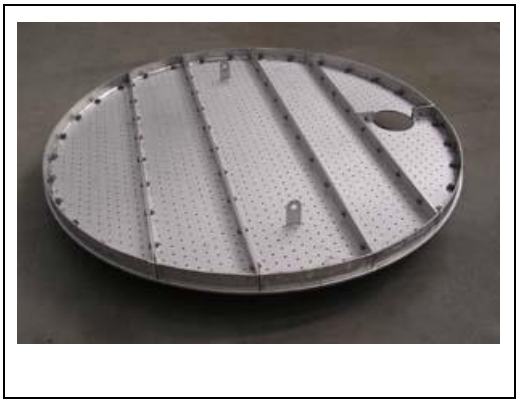

Figure 10. Commercially used sieve sparger

a. Porous

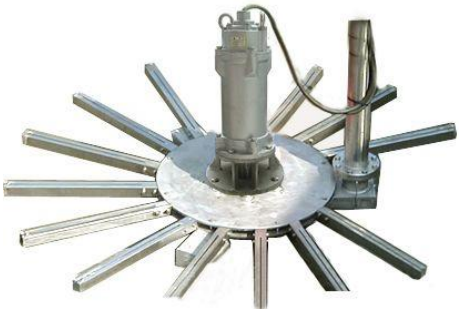

b. Radial

c. Spider

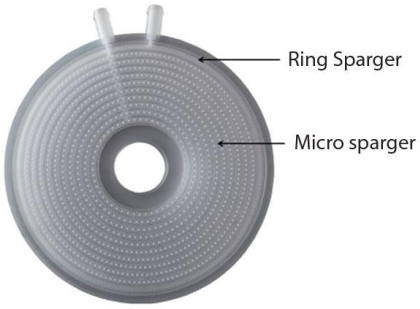

d. Ring sparger (De Wilde et al., 2014)

Figure 11. Different types of sparger used commercially

2.3.5. Gas transfer

During gas transfer, CO_2 needs to be added and oxygen needs to be removed from the medium in the PBR system, and therefore is considered an important aspect of PBR design (Huang et al., 2017). A high aeration rate might damage microalgae cells due to mechanical stress as well as increase running cost (Cañedo and Lizárraga, 2016). CO_2 and pH have an inverse relationship, and therefore, CO_2 and its flow rate should be adjusted accordingly to maintain proper pH in the medium (Wang et al., 2012). CO_2 introduced into the PBR through a sparger is distributed within the medium by bubbles.

2.3.6. Light

When the temperature control, nutrients, and mixing are not the limiting factors then light intensity, availability and its duration play a significant role in photosynthesis and the growth of the microalgae (Al-Qasmi et al., 2012; Lee and Low, 1992). The absorption spectra of microalgae and cyanobacteria range from 400-700nm (Berberoglu et al., 2007b) and the photosynthetic apparatus that can accommodate the maximum light intensity (Saturation light Intensity) varies from 50-200µmol photons (PAR) $m^{-2}s^{-1}$ depending upon the species (Goldman, 1979). It is considered that the light spectrum above 750 nm wavelength does not have sufficient energy to be converted into chemical energy. The absorbed energy by chlorophyll from low energy photons can only be converted into heat. To high energy is when the light wavelength is below 350 nm, and this will lead to photo oxidation. Thus, the spectral range of 350-750 nm is good for photosynthesis (Kommareddy and Anderson, 2003b). The light energy spectrum range of 600-800 nm is required to obtain a high hydrogen production rate and is considered as the actual photon range needed for the photosynthetic process (Uyar et al., 2007). Therefore,

when determining the light requirement in a PBR, care should be taken as to what light sources are used with respect to intensity and light spectrum. The relationship between light spectrum wavelength and energy is provided in equation (1).

$$E = \frac{hc}{\lambda} \quad (1)$$

Where E= energy of quanta (J/quanta), h=Planks constant (6.626 $*10^{-34}$ J.s), c=speed of light (2.998$*10^{8}$ m/s) and λ =wavelength of the photon (m) (Sheppard et al., 2006). To overcome the effect of light inhibition and light saturation either the light path should be decreased or proper mixing should be done. The concept of the surface to volume ratio (SVR) has been introduced. The favorable SVR will be obtained by selecting the appropriate geometries of PBR that reduce the light path length and reduce the mixing energy. If SVR is high, then the cell production is high, and the volumetric productivity is high as well.

2.3.7. Light intensity

Light intensity and growth rate show a linear relationship but reports indicate that the correlation doesn't predict performance when scaling up a PBR though (Ogbonna et al., 1995). Authors have also claimed that the attenuation coefficient is a good PBR scale up factor. Various mathematical models have been developed by researchers based on the Lamberts law for light distribution and irradiance profile estimation so that proper light distribution and intensity could be supplied to the culture by minimizing mutual shading (Katsuda et al., 2004; Molina Grima et al., 1994). While some researchers claim that Beer-Lambert law cannot be used to predict the irradiance inside the photobioreactor

because it ignores light scattering (Berberoglu et al., 2007a). They developed a new model. The linear relationship between the extinction coefficient and biomass concentration/dilution (β_X) factor has been developed as $\beta_X = 360.30X \; at \; 683 \; nm$ where, β_X = extinction coefficient, m−1 and X= microorganism concentration ranging from 0.04 to 0.35, kg dry cell mass/m^3 (Berberoglu et al., 2007a). This equation helps us to predict the extinction coefficient at certain biomass concentration. Table 7 and Table 8 shows the models developed for estimating light intensity and light irradiance along with attenuation coefficients to be used in the model.

Table 7. Light attenuation coefficient

Species	Attenuations coefficient	Remarks
Anabaena	5.2×10^{-6} cm^2 $filament^{-1}$	(Litchman, 2003)
Phormidium	1.7×10^{-6} cm^2 $filament^{-1}$	
P. tricornutum	0.0369 m^2/g	(Molina et al., 2001)
Chlorella pyrenoidosa	0.200m^2/g	(Ogbonna et al., 1995)

Table 8. Different formula used by researchers to find the light intensity and irradiance

Developed model for estimating light intensity and radiation	Remarks
$I(\lambda)=I_o(\lambda).\ Exp(-Ka(\lambda).p.C)$ I(λ)= Light Intensity Ka(λ)=extinction coefficient for biomass at wavelength λ C=Biomass Concentration I_o (λ)=Intensity of the light source at wavelength λ	(Molina Grima et al., 1994)
$I_{av} = \frac{I_o}{\Phi_{eq} K_a C_b}[1 - \exp(-\Phi_{eq} K_a C_b)]$ Iav= Average Light Intensity I_0= Intensity at the culture surface Qeq=path length from the surface to point in the growth Ka=extinction coefficient for biomass C=Biomass Concentration	(Alfano et al., 1986), (Molina et al., 2001)
$I = \frac{Lo^2}{(L+Lo)^2} \sum_{\lambda} I_{0,\lambda} . 10^{-\in c_{ell,,\lambda}\ CL}$ I= Light Intensity L=Light path length L_0=Distance from the light source to the illuminated surface I o, λ =Intensity of the light source at wavelength λ $\in c_{ell,,\lambda}$ = Extinction coefficient of the cell at wavelength λ C=Biomass Concentration	(Katsuda et al., 2004)
$\vec{s}\frac{\partial I\lambda(z,\vec{s})}{\partial z} = -K_{eff,\lambda}\ I_\lambda(z,\overrightarrow{s})_- \sigma_{eff,\lambda} + \frac{\sigma_{x,\lambda}}{4\pi}\int 4\pi I_\lambda(z,\overrightarrow{s})\Phi_{x,\lambda,}(\overrightarrow{s_i},\overrightarrow{s})\frac{\sigma_{x,\lambda}}{4\pi} d\Omega i + \frac{\sigma_{B,\lambda}}{4\pi}\int 4\pi I_\lambda(z,\overrightarrow{s})\Phi_{B,\lambda,}(\overrightarrow{s_i},\overrightarrow{s})$ $I\lambda(z,\vec{s})$ = Radiation intensity in direction s at z location Keff = Effective spectral absorption coefficients $\sigma_{eff,\lambda}$ = Effective scattering coefficients $\Phi_{x,\lambda,}$= Scattering phase functions of bacteria $\Phi_{B,\lambda,}$= Scattering phase functions of bubbles	(Berberoglu et al., 2007a)

2.4. Different Sources of artificial light

Sun Light

Open pond PBRs and closed PBRs operated in the outdoor environment use sunlight for photosynthesis. The incident solar radiation in the central daylight time zone can exceed 2000µmol photons $m^{-2}s^{-1}$ which is significantly greater than the 200µmol photons $m^{-2}s^{-1}$ required for photosynthesis **(**Tredici and Zittelli, 1998**)**. Sunlight as a light source is employed in industrial applications because of its cost-effectiveness (low cost). However, sunlight intensity varies throughout the day making a sunlight dependent PBR ineffective. To overcome this problem, artificial lighting systems were introduced to achieve consistent and continuous illumination. An artificial lighting system should be designed to provide optimum energy. Table 9 provides data for several artificial light sources used in PBR systems

Fluorescent Lights

Researchers started using fluorescent lamps for growing microalgae in PBRs. Light emitted by fluorescent lights is in the visible region. The efficiency of fluorescent lamps is up to 45%, Table 9. It is the most commonly used light source because it is inexpensive, readily available, easy to install, and easy to control. The emitted light is diffuse and reflectors are required to direct the light into the PBR. Light intensity tends to decrease after a year. Therefore, other light sources are explored.

LED Lights

LEDs are a unique type of semiconductor diode consisting of p-n junctions in which current flows from p to n side of the diode and not in the reverse direction (Carvalho et

al., 2011). It emits light in a narrow wavelength band. Chlorophyll light absorption is strongest in the red and blue portions of the PAR region. The light outside of the red and blue band tend to be absorbed and converted to thermal energy or be reflected rather than being used in the photosynthesis process. Therefore, LED light in a narrow red wavelength band produces less heat than other light sources tested (Kommareddy and Anderson, 2003b; Matthijs et al., 1996). Several lights such as cool white lights, fluorescent lights, Gro-Lux lights, incandescent lights, halogen lights, and LED lights are used in PBRs for microalgae production. AllnGaP II (aluminum indium gallium phosphide) LEDs emit light in the wavelength range of 600-700 nm and can be up to 98% efficient in converting electrical energy to photon energy, Table 9. Research studies have shown that cell size of cultures grown in red LED light (25-35 μm^3/cell) is smaller than that grown in fluorescent light (50-120 μm^3/cell) (Lee and Palsson, 1996). However, the concentration of biomass (g/l) was found to be similar from the two light sources.

Different led lights are available and can be used to grow microalgae (Koc et al., 2013). However, the light sources significantly affect microalgae growth rate and biomass concentration for example, red light intensity produces smaller cells than blue light whereas blue lights yield bigger diameter cells but with less total weight than red light (Shu et al., 2012).

Acrylic (Plexiglas) and LED light

Internal illumination is often required when a PBR is scaled up or when the biomass produced creates sufficient mutual shading to reduced light intensity to the point where photon flux is insufficient to maintain photosynthesis. Shading in the PBR increases with

increase in biomass concentration, Figure 12. However, it also increases due to bubble flow, and bubble size in the PBR and the length of the light path. Internal illumination overcomes shading issues but it increases the cost of production (Ogbonna et al., 1996).

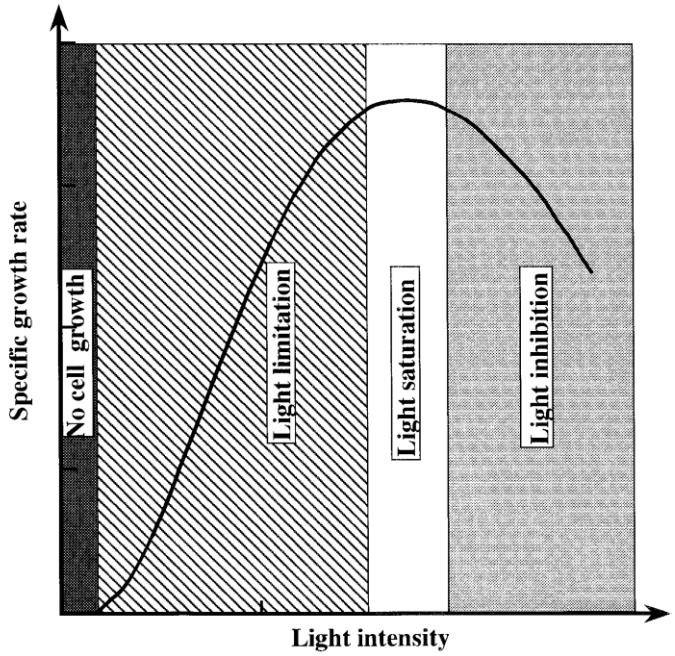

Figure 12. Light intensity versus growth rate of photosynthetic cell (Ogbonna and Tanaka, 2000)

Researchers are interested in increasing the light transmission efficiency into the interior less well-lit regions of the PBR by using light guides. These light guides are made of plexiglass, and are generally of rod-shape (Pozza et al., 2012). Plexiglas PBR walls help to diffuse the light when the light is supplied by a LED source (Pozza et al., 2012). Kommeraddy et al. studied light guides which were made by cutting acrylic rod with a band saw and lathe (Kommareddy and Anderson, 2003a). The cut surfaces were finished with a belt sander and buffed using the red coloring compound. A LED panel was used as the light source with a light guide positioned directly in front of one LED light.

Table 9. Different light sources and it's properties (Kommareddy and Anderson, 2003b)

Light sources	Total light between 400-500 nm and 600-700 nm (%)	Intensity $W/m^2/nm$	Advantages	Disadvantages
Fluorescent	45.65	5.720	• Low initial cost	• lights are emitted in all directions. Therefore, reflector are required to direct the light • light intensity decreases after 1 year
Gro-Lux	56.87	3.603	• % of total light intensity on 600-700 nm is higher than the Fluorescent	• Similar to Fluorescent Lamp
Incandescent	4.28	5.085	-	• Only 2.8% of the photons emitted by this by this light source are usable
Halogen	3.60	0.785	-	• Produce less photons • Hot and inefficient
LED	87.59-98.38	(14.229-41.641)	• Provide peak wavelength, • Cost effective • High Luminous efficiency • Long life span • Light intensity can be varied easily by varying the power	• Initial expenses is high
Plexiglas	-	310-625 lux	• Increases the light transmission efficiency	• High capital cost, harvesting cost is high

The study found that light guides with finished and polished surfaces transmitted (625 lux) more light then light guides with the least finished/buffed surface (Kommareddy and Anderson, 2003a). Table 9 shows a summary of light sources, their intensity, advantages, and disadvantages as light sources in a PBR application.

2.5. Harvesting

Harvesting of microalgae means concentrating microalgae from the diluted algae growth medium. It is an important part associated with the cost of biofuel production from microalgae. Studies have found that harvesting process of microalgae accounts 20-30% of the total cost of converting it into biofuel (Grima et al., 2003). Harvesting of microalgae cells depends upon its size, density and the value of the target products (Brennan and Owende, 2010).

2.6. Types of Harvesting Technologies

2.6.1. Filtration

Filtration is a method suitable for large size microalgae. Filtration process has been found successful in the recovery of large algae cells. Filtration involves running the medium with algae through filters on which the algae will accumulate and allow the medium to pass through the filter (Figure 13). The medium is continuously run through the micro-filters until the filter collects a thick algae paste. Low-cost filtration is often used to harvest filamentous algae (Christenson and Sims, 2011).

Figure 13. Microalgae harvesting using filtration technique.

Vacuum filtration is usually employed for large particle size. To obtain the higher recovery for small size microalgae ultra-filtration is preferred (Pragya et al., 2013). Membrane filtration is simple and reliable, but its not very effective for dilute concentration. This method is suitable for small systems and works efficiently if the culture is preconditioned to 3-4% biomass on mass basis (Becker, 1994).

2.6.2. Flocculation

Since algae are in suspension, the algae should be flocculated or screened first. Flocculation is the process of solute aggregation resulting from joining of solutes present in algae growth medium. Even though this method is quite expensive, it has been considered as one of the low-cost methods for harvesting microalgae (Benemann and Oswald, 1996). Different types of flocculation are explained as below-

2.6.2.1. Auto flocculation

It is the natural process of flocculation and generally, carried out in the lab. Auto flocculation is slow and unreliable, and cannot be applied to all microalgae species

(Milledge and Heaven, 2013). To auto flocculate the CO_2 supply should cut off to stop mixing and minimize algae suspension. Restricting CO_2 supply causes depletion of CO_2 in the PBR which increases pH making medium more basic. As a result, calcium hydroxide and magnesium hydroxide precipitates are used to cause setteling of the microalgae. Settled algae separate from the medium and the liquid is slowly removed from the reactors . Harvesting of cells along with flocculation is one of the successful harvest methods, but this method alone is not sufficient to achieve high recovery. Thus, it needs to combine with other separation methods to achieve higher cell recovery.

2.6.2.2. Chemical flocculation

This flocculation method is often used for harvesting microalgae. It is considered as one of the cheapest methods but is used as pretreatment because the size of microalgae is very small. To flocculate and coagulate the cells, electrolytes and synthetic polymers are used. Aluminum and ferric cations, aluminum sulfate, and ferric chloride are often used for charge neutralization because of the +3 charge (Shelef et al., 1984). When these chemicals react with the calcium bicarbonate present in the medium or waste water, the product obtained is normally hydroxides like Aluminium hydroxide and ferric hydroxide. These hydroxides settle through the medium separating the biomass from the liquid as shown in Figure 14 (Ebeling et al., 2003). Some cationic polymers have been proven effective like chitosan, cellulose, surfactants, cationic polyacrylamides and some artificial fibers (Bilanovic et al., 1988). The major disadvantage of this separation method is the removal of chemicals from the separated algae which makes it inefficient and expensive for commercial use, though it may be practical for lab use (Chen et al., 2012).

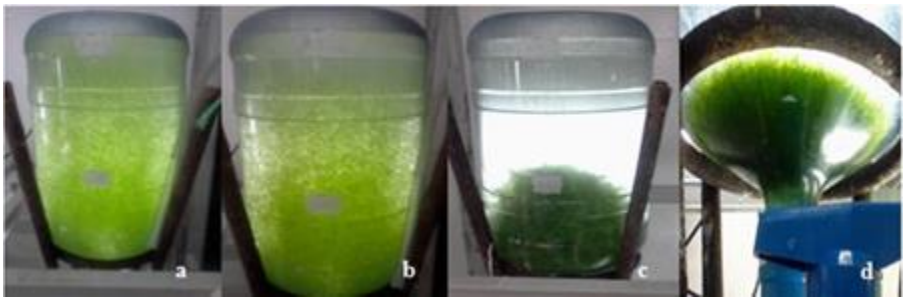

Figure 14. Chemical Flocculation process starting at a and compete at d. (Low and Toledo, 2015)

2.6.3. Centrifugation

Centrifugation is one of the best methods used by many researchers, manufacturers, and institutions. It uses centrifugal force to separate microalgae from the medium. Almost all types of microalgae can be separated by this method. Recovery achieved from this method is greater than 90% through centrifugation process, but it is dependent on the flow through put (Park et al., 2011). This method is one of the efficient methods but it is very energy intensive which makes it costly and economically infeasible at large scale (Rawat et al., 2011).

A large volume of culture consumes a lot of time, and its exposure to high gravitational and shear force can damage the algae cell (Chen et al., 2011). The centrifugal force causes relatively dense materials to settle down more quickly than they would under normal gravitational force. Figure 15 shows the example of separation of micro algae through centrifugation process.

Figure 15. Harvesting micro algae through centrifugation process. (Dayan et al., 2010)

2.7. Challenges in Production and Harvesting

Despite of lot of advantages of microalgae in biofuel there are still lot of challenges encountered with the production and harvesting (Griffiths et al., 2011). The overall challenges in microalgal biomass is the economic recovery. Some of the problems associated with the large-scale microalgae production and harvesting are-

- Cost of the PBR is very high, 50% of the total capital cost is from the PBR.
- Scale-up problems due to complex design consideration.
- Harvesting of microalgae is challenging because microalgae are very dilute. Normally microalgae have a solid concentration ranging from 0.5- 4 g/L and its size is very small ranging from 1 to 30 μm.

3. MATERIAL AND METHODS

3.1. Material and Energy Balance

3.1.1. Material Balance

A material balance was performed to estimate the amount of nutrient required to produce 1000 g of algal biomass. Anabena with elemental composition of $C_{44.6}H_7O_{25}N_{7.68}P_{0.9}S_{0.3}$ was used for estimating the nutrients required for its cultivation and biomass production (Krivtsov et al., 1999). Anabena was grown in BG11 media and therefore, elemental compounds of BG11 media (the major nutrients in the compounds are $NaNO_3$, K_2HPO_4, and $MgSO_4$) was used to develop the stoichiometric equation to balance the elements of Anabena biomass and is represented by the photosynthetic reaction presented in equation (2).

$$44.6CO_2 + 7.68NaNO_3 + 0.9K_2HPO_4 + 0.3MgSO_4 + 8.09H_2O \rightarrow$$
$$C_{44.6}H_7O_{25}N_{7.68}P_{0.9}S_{0.3} + 7.68NaOH + 0.3\ Mg\ (OH)_2 + 1.8KOH + 44.025O_2 \quad (2)$$

The total atomic weight of biomass composition was calculated by summing up the atomic weight of individual elements of the biomass. Atomic weight of each individual element was calculated by multiplying the atomic mass of the individual element with the number of moles present in the biomass composition. A similar procedure was adopted to compute the total atomic weight of BG11 compounds. With the help of the atomic weight of biomass and BG11 compounds, the amount of N, P, S, and CO_2 required to produce 1 g of biomass were calculated using simple unitary methods.

3.1.2. Energy Balance

To compute the energy of a photon equation (1) was used. Considering 10 photons are required to fix 1 carbon atom, total carbon atoms per mole of biomass was calculated. Therefore, the amount of energy to fix a carbon atom in 1 mole ($C_{44.6}H_7O_{25}N_{7.68}P_{0.9}S_{0.3}$) of biomass was found by multiplying the total number of carbon atoms in a mole of biomass by the energy of a photon.

Standard molar enthalpies for BG11 compounds and biomass composition were obtained from different literatures and are presented in Table 10 (Luff and Reed, 1978; Silberberg, 2007).

Table 10. Standard Molar enthalpies of formation of different compounds.

Compounds/elements	Standard Enthalpies (KJ/mol)	Remarks
O_2	0	(Luff and Reed, 1978; Silberberg, 2007)
CO_2	-393.5 KJ/mol	
H_2O	-241.8 KJ/mol	
$NaNO_3$	-446.2 KJ/mol	
K_2HPO_4	-376.1 KJ/mol	
$MgSO_4$	-1278.2 KJ/mol	
NaOH	-469.6 KJ/mol	
$Mg(OH)_2$	-924.7 KJ/mol	
KOH	-424.76 KJ/mol	
Biomass	-22.5KJ/g for Nannochloropsis sp	(Vree et al., 2015)

Standard enthalpies for each BG11 compounds and elements of Anabena were multiplied with their corresponding mole number to obtain the enthalpies of reactants and products as presented in Table 10. Finally, the change in enthalpy of reaction was computed by subtracting the sum of all enthalpies of reactants from the sum of all enthalpies of products as given by equation (3).

$$\Delta H = \sum H_{products} \quad - \sum H_{rectants} \tag{3}$$

Where, ΔH is change in enthalpy of reaction at constant pressure, $H_{products}$ is enthalpy of formation of products and, $H_{rectants}$ is the enthalpy of formation of the reactants.

3.2. Light Analysis

Light data from previous lab work was used to see the effect of flowrate and path length (depth of photobioreactor) on light intensities. The experiment was performed at lab scale using a flat plate PBR made up of acrylic sheets. The sparger was placed at the bottom of the PBR and illumination was red LED light at 656 nm. Illumination was done on one side of the PBR while light intensity was measured on the other side of the PBR. Light intensities were measured under three diferent conditions. The first one was at different path lengths which were 101mm (4”), 152mm (6”), 203mm (8”), 254mm (10”), and 305mm (12”), the second one was at different air flow rates ranging from 1 to 10 LPM, and the third one was at different biomass concentration ranging from 0 kg/m^3 to 1 kg/m^3 with an interval of 0.1 kg/m^3 (Rajendran, 2016). A randomized block design test was performed to compare means of five different treatments (path lengths). The null hypothesis for the t-test assumed that all means are equal and is given by equation (4) and the alternative hypothesis assumed that at least one mean is different and is given by the equation (5).

$$\mu_0 = \mu_{pathlengh\ 102mm} = \mu_{pathlengh\ 152mm} = \mu_{pathlengh\ 203mm} = \mu_{pathlengh\ 254mm} = \mu_{pathlengh\ 305mm} \tag{4}$$

$$\mu_b = atleast\ two\ of\ the\ mean\ is\ not\ equal \quad (5)$$

Tukey Honest Significance Difference (HSD) test was performed to check which specific groups of path lengths and which specific groups of flow rates were significantly different from each other. This test is generally performed when the randomized block design test and ANOVA test shows the significant result. To compute the test, HSD is calculated using the equation (6)

$$HSD = \frac{M_i - M_j}{\sqrt{\frac{MS_w}{n_h}}} \quad (6)$$

Where,

M_i-M_j=means difference between two groups

MS_w=Mean square within the groups

n= number of group in a treatment

Similarly, regression analysis was used to verify the relationship between the dependent variable (light intensity) and independent variables (flow rate and path length). The analysis was performed at 95% confidence level ($\alpha = 0.05$). The light data used in this research is presented in Table 11.

Table 11. Light Intensities at different path length and flow rate (Rajendran, 2016)

Light Intensity (μmol m^{-2} s^{-1})					
Flow rate (liters/min)	Depth of Photobioreactor (path length)				
	102mm	152mm	203mm	254mm	305mm
	(4")	(6")	(8")	(10")	(12")
0	89.53	78.56	66.97	62.66	58.66
1	83.23	77.18	63.3	53.13	52.38
2	75.52	72.67	59.63	52.4	48.74
3	72	70.07	58.01	51.21	47.6
4	68.44	67.49	57.65	50.14	46.68
5	67.03	64.46	53.52	49.19	45.81
6	61.24	62.37	55.13	49.16	40.95
7	64.13	60.33	53.88	48.73	42
8	60.1	57.64	50.83	48.87	40.95
9	60.23	56.02	51.69	48.11	39.28
10	56.62	54.24	50.34	48.99	39.58

3.3. Sparger Design

Sparger design was carried out using an analysis software named as “SPARGER”, which was developed on a Java platform. The software simulates three different models, named as Static regain, Acrivos, and Pressure drop method. The input parameters for the simulation are input air flow rate, input air pressure, height of liquid, sparger diameter, hole diameter, hole discharge coefficient, length of sparger, and number of rows of holes. This software can simulate the data in SI and English Units. The value of input parameters used for designing the sparger are listed in Table 12.

Table 12. Inputs for the sparger simulation

Input variables	Inputs
Diameter of Sparger (cm)	1.27
Discharge (m^3/sec)	0.000197
Pressure (Pa)	7985
Length of pipe (cm)	121.92
Discharge coefficient	0.625
Diameter of hole (mm)	0.08
Type of liquid	water
Simulation model	Acrivos

The output obtained from the analysis includes number of holes, pitch distance, percentage of gas remaining at the last hole, ENU, and a check for weeping. Apart from this, it also provides graphs of hole gas flow rate, and sparger gas flow rate. Also, the tabulated results are the number of holes and the respective hole velocities, gas hole flow rate, sparger velocity, sparger flow, sparger velocity pressures, static pressures, and total pressures.

The major parameters calculated employed by the software for simulation include critical velocity, ENU number estimation, and % of air remaining. ENU is the indication of all the air leaving the sparger along its length and tries to keep the same air flow rate through all the holes in the sparger

Critical velocity can be calculated using equation (7). If the orifice velocity is greater than the critical velocity then the sparger is not weeping.

$$V_c = \sqrt{1.1 * 0.44(\rho_l - \rho_G) * d_o g * (\frac{L}{d_o})^{-0.12} * (\frac{\Delta x}{d_o})^{-0.145} * (\frac{H_l}{d_o})^{-0.67}} \quad (7)$$

Where, V_C is the critical velocity (m/s), ρ_L is density of the liquid (kg/m^3), ρ_g is density of the gas (kg/m^3), d_o is the diameter of sparger , L is the length of sparger (m), Δ_x is the pitch length (mm), g is the acceleration due to gravity (m/s^2)and, H_l is the height of the liquid (m).

Similarly, ENU was calculated using equation (8)

$$ENU = \left(\frac{Last\ hole\ velocity - First\ hole\ velocity}{First\ hole\ velocity}\right)^{*}\ \ 100 \tag{8}$$

Finally, the percentage of air remaining in the last hole is calculated using equation (9)

$$\%\ Air\ remaining = \frac{\text{gas flow in the tube after the last holes}}{\text{input gas flow in the tube}} * 100 \tag{9}$$

3.4. Bubble study

The designed sparger was used to test the flow patterns of the bubbles sparged into the 160 L PBR. PVC pipe of 0.5-inch (1.27 cm) diameter and 48- inch (121.92 cm) length had drilled with 30 holes drilled into it using hole driller with a hole diameter of 1/32 (0.079 cm) inch at a spacing of 1.59- inch (4.039 cm). A rectangular flat plate PBR of 0.325-inch (0.826) thick acrylic sheet was used to construct the PBR tank with dimensions of 50- inch (127 cm) in length, 6-inch (15.24 cm) in width, and 40- inch (101.60 cm) in height. A sparger was fixed at the bottom of the PBR to allow upward flow of gas through the PBR. An air flow meter was placed just before the sparger to check the flowrate of air. To create the bubbling effect, air was introduced through the sparger with flowrates of 10, 20, 30 and 40 LPM. The performance of sparger was tested under two different conditions. The first tests were varying water levels in the PBR and adjusting the height over the range of 5,

10,15, 20, 25 and 30-inch. The second one was the number of sparger tubes 1, 2, 3, and 4 in the PBR.

3.5. Cyanobacteria Cultivation

Cyanobacteria culture was prepared from 5 ml of Anabena 7120 species sample obtained from the Microbiology Department at SDSU. Before transferring it to any media, the strain was checked under the microscope to check for any contamination in the culture. This was performed by grabbing 1µl of sample from the collected culture and placing it on a microscope glass slide. The sample on the glass slide was cautiously covered with cover slip avoiding any trapping air and/or dust particles before placing it under the microscope. A compound microscope with an objective lens of 40X was used to capture the image. Infinity Analyzer software was used to capture the image of the cultivated strain in the computer directly from microscope, Figure 16.

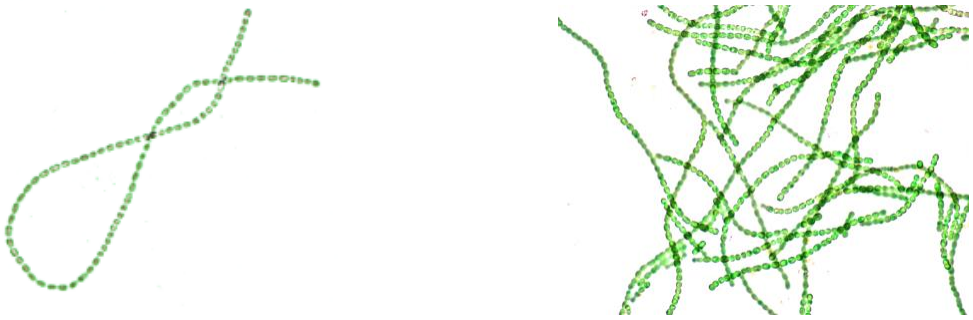

Figure 16. Anabaena 7120 strain capture through 40X optical lens before transferring it to 1L media (left) and after 1 week (right)

After testing for any contamination, the culture was transferred to 1L of BG11 media prepared in a 2L glass bottles. BG 11 media was prepared in the lab using the compositions presented in Table 13.

Table 13. Composition of BG 11 media (Stanier et al., 1971)

Chemicals	Amount per liter	Trace metal mix	
		Chemicals	Amount per liter
$NaNO_3$	1.5g	H_3BO_3	2.86g
K_2HPO_4	0.04g	$MnCl_2{\cdot}4H_2O$	1.81g
$MgSO_4{\cdot}7H_2O$	0.075g	$ZnSO_4{\cdot}7H_2O$	0.222g
$CaCl_2{\cdot}2H_2O$	0.036g	$NaMoO_4{\cdot}2H_2O$	0.39g
Citric acid	0.006	$CuSO_4{\cdot}5H_2O$	0.079g
Ferric ammonium citrate	0.006	$Co(NO_3)_2{\cdot}6H_2O$	49.4mg
EDTA	0.001	Distilled water	1L
Na_2CO_3	0.02		
Trace Metal mix	1 ml		
Distilled water	1L		

To prepare BG11 media, purified water was used to avoid any contamination in the media. Water purification was done using Thermo scientific Barnstead EASYpure RoDi ultrapure water purification system. Further, the prepared media was sterilized by placing it into autoclave for 20 minutes at 121°C. The sterilized media was then cooled to room temperature before the culture was added. Gas was supplied to the culture container to keep micro-alage in suspension using an electrical air pump connected to a small glass rod. Fluorescent light was used for illumination at 43 watts to meet the light demand of cyanobacteria. The lab cultivation of anabenea in 2L glass bottle is presented in Figure 17.

Figure 17. Anabeana 7120 grown in 2L glass bottle.

3.5.1. PBR setup for the growth of Anabaena

The materials and dimensions of the PBR and sparger were the same that were used to study the bubble flow patterns. Figure 18 shows the set up of a flat plate PBR system in the laboratory filled with 132L BG11 media. The cyanobacteria grown in 1L BG11 media was then transferred to the PBR. Four spargers were used to supply the gas mixture at the bottom of the PBR parallel to the length of PBR. Flowmeters for air and CO_2 gas was placed before the plenum. The flowmeters were used to regulate the flow of air and CO_2 into the PBR. The gas mixture coming out of the flowmeters was delivered to the plenum and is supplied to the sparger that was connected to it by a 0.25-inch (0.635 cm) tube. The purpose of the plenum was to distribute the gas mixture supply evenly to all four spargers. The air flow rate and CO_2 flow rate was adjusted based on the pH of the media.

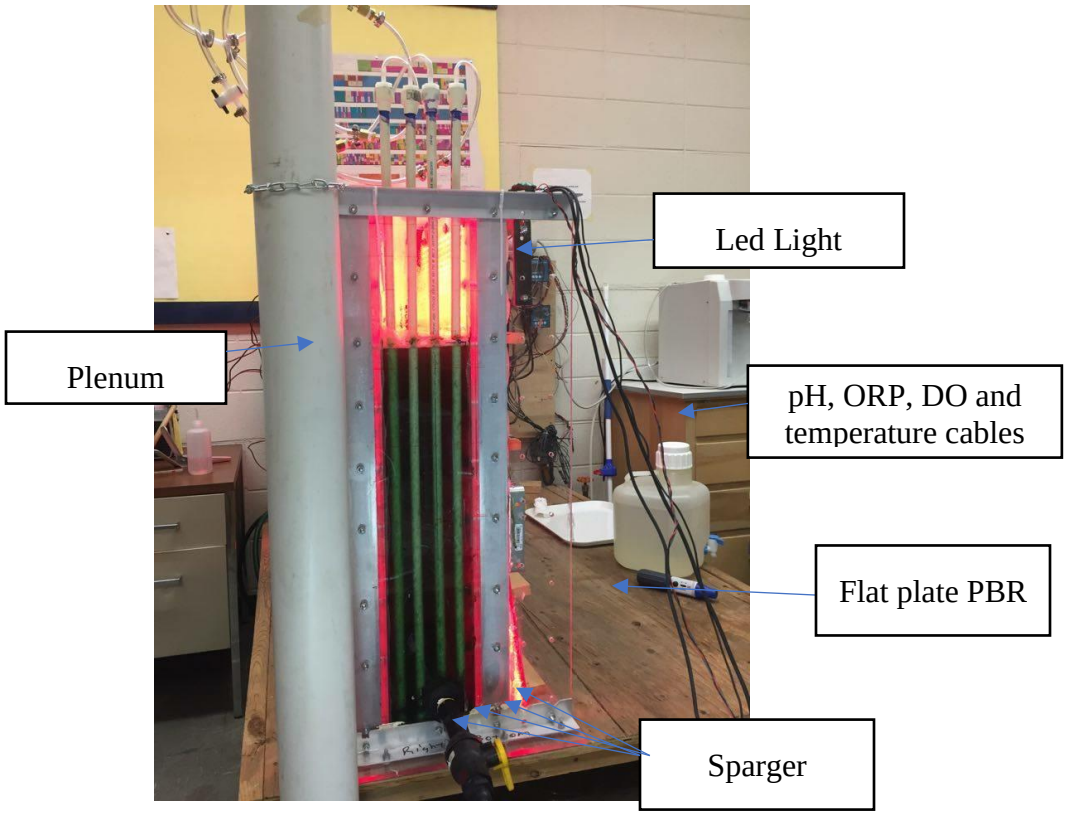

Figure 18. Anabena 7120 growing in 132 L Flat plate PBR.

3.5.1.1. Instrumentation

Physical parameters such as pH, ORP, DO and temperature were monitored during the experiment. The instrument probes which were connected to a transmitter were placed inside the PBR media. Eutech Instruments αlpha pH 500 two-wire transmitter was used to measure pH and ORP (mV) whereas αlpha DO 500 two-wire transmitter was used to measure DO (mg/L) and temperature (^{0}C). Eutech Instruments 971944 Galvanic DO probe, 0 to 20 ppm, with a 10ft (3.048 m) cable was used for monitoring the DO and a Cole Parmer flat surface ORP and pH electrodes were used to monitor ORP and pH respectively (Figure 19). A program written in National Instrument Lab view 8.5 software was used to acquire the data from the transmitters and record the data.

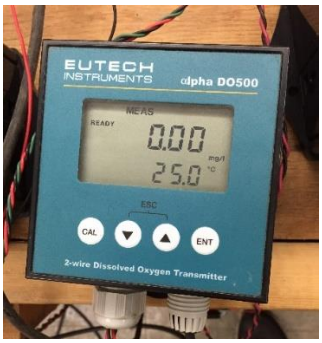

Figure 19. Transmitter used for DO

This software acquired readings every second from the transmitters. However, the daily average was determined for the analysis. Daily average value was used in the analysis because biomass concentration was not recorded every second and the sample number of biomass versus the physical parameters will be different while performing the statistical analysis.

3.5.1.2. Biomass measurement

The experiment was run for 22 days and the biomass measurement was recorded every 12 hours. A volumetric pipette was used to withdraw 100 ml sample from the growing media. Then the average biomass on a daily basis was calculated to compare the values with the 13L reactor. Cyanobacteria biomass was then separated from the sample using vacuum filtration equipment. The concentrated biomass was collected using Whatman filter paper (number 4) with a diameter of 40mm and the pore size of 20-25µm. In every sample, the biomass collected on the filter paper was weighed using a Thermo scientific 4 digit weighing balance to record initial weight and then placed in hot air oven at 70 to 80°C for 10 hours to dry the biomass. The oven dried biomass was again weigh after 10 hours and the final weight was recorded. Figure 20 shows the oven dried biomass

samples ready for taking final weight. The weight of the biomass was calculated using equation (10).

$$Weight\ of\ biomass\ \left(\frac{g}{L}\right) = \frac{\text{Final weight (g)} - \text{Initial weight (g)}}{100\ (\text{ml}) * 1\ (L)} * 1000\ (L) \quad (10)$$

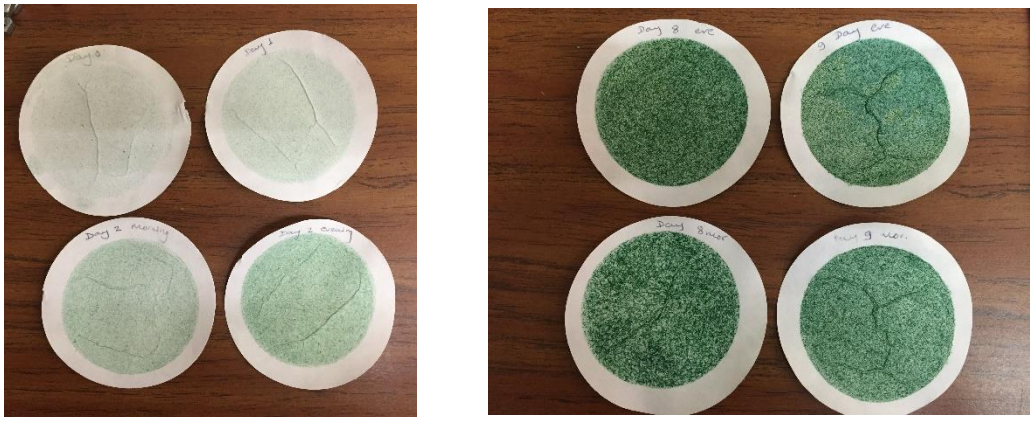

Figure 20. Biomass concentration ready to take the final reading.

3.5.1.3. Light setting

Red LED light having a wavelength of 650 nm was was used for illuminating the PBR. One light panel consists of a 24 x 36 LED matrix. Four sets of light panels were provided to meet the light requirement of the system. On each side of the PBR, two sets of light panels were providede in which each set were connected in parallel (Figure 21). A total of four control units were installed to supply power to the light panels from a power supply with a constant voltage of 13V and constant current of 30A.

Figure 21. Red LED light set up

3.6. Result Analysis

3.6.1. Regression analysis

Regression analysis was performed using R programming to model the relationship between the dependent variable (biomass) and independent variables (pH, DO, ORP, and temperature). Also, regression analysis was performed for the dependent variable (biomass) and independent variables (CO_2 flow rate and air flow rate). In order to check at the larger margin of error and therefore, statistical significance was tested at 95% confidence interval. This means that there is a 95% probability that the confidence interval will cover the true population mean. The multiple linear regression equation is represented as in equation (11) (Tranmer and Elliot, 2008).

$$Y = \beta_0 + \beta_1 X_{1i} + \beta_2 X_{2i} \ldots\ldots\ldots + \beta_p X_{pi} \quad (11)$$

Where, Y= Dependent variable; β_0= Slope; β_1 to β_p are the coefficients with respect to the dependent variables X_1 to X_p.

3.6.2. Student's t-test

Student t-test was performed using Microsoft excel to check the difference between mean biomass production in 13L and 132L bioreactor. Since, the number of samples of observation in two experiments were different, two-sample t-test for unequal variance was used (Ruxton, 2006). For two sets of observation with mean μ_1 and μ_2, variances s_1^2 and s_2^2 and sample sizes N_1 and N_2, the t-statistic of unpaired student's t-test is computed using equation (12):

$$t = \frac{\mu_1 - \mu_2}{s_p^2 \sqrt{\left(\frac{1}{n_1} + \frac{1}{n_2}\right)}} \tag{12}$$

Where, s_p^2 is the pool variance and is calculated using equation (13).

$$s_p^2 = \frac{(n_1 - 1)s_1^2 + (n_2 - 1)s_2^2}{n_1 + n_2 - 2} \tag{13}$$

For student's t-test the degree of freedom is calculated using equation (14) (Moser and Stevens, 1992).

$$v = \frac{\left(\frac{1}{n_1} - \frac{u}{n_2}\right)^2}{\frac{1}{{n_2}^2(n_1 - 1)} + \frac{u}{{n_2}^2(n_2 - 1)}} \tag{14}$$

$$u = \frac{s_1^2}{s_2^2} \tag{15}$$

4. RESULTS AND DISCUSSIONS

4.1. Mass Balance and Energy Balance

4.1.1. Mass Balance

Mass balance is an important step in algal biomass production in a controlled environment. It was performed to estimate amount of nutrient consumption by the cyanobacteria for its growth and biomass production. The mass balance follows the simple approach of balancing chemical equations and calculating atomic weight of each reactant and product. The atomic weight of one mole of microalgae with molecular formula $C_{44.6}H_7O_{25}N_{7.68}P_{0.9}S_{0.3}$ was calculated as 1087.617 g and the atomic weight of BG11 media prepared using compounds $NaNO_3$, K_2HPO_4, and $MgSO_4$ were calculated as 652.759 g, 156.758 g, and 36.110 respectively (Krivtsov et al., 1999). The detail calculation of atomic weight of each compound and nutrient required to produce 1 gm of algal biomass is presented in Appendix 1 and Appendix 2. From the atomic weight of each compound, the quantity of nutrients required to produce 1 gram of biomass were calculated.

Table 14. Amount of nutrient required to produce 1g of biomass

Nutrients	**Amount required to produce 1g of biomass (g)**
Nitrogen	0.099
Phosphorous	0.026
Sulphur	0.009
Carbon	0.493
Magnesium	0.007
Sodium	0.160

The major nutrients required for algal biomass production are: Nitrogen (N), Phosphorous (P), Sulphur (S), Carbon (C), Magnesium (M), and Sodium (Na). The

amount of each nutrient required to produce 1g of algal biomass is presented in Table 14. From the calculations, it was found that the highest quantity of nutrients required to grow cyanobacteria (algal biomass) was Carbon followed by Sodium, Nitrogen, Phosphorous, and Sulphur.

4.1.2. Energy Balance

An energy balance was performed to determine the net energy required for the production of biomass under controlled environment conditions. The detail calculations of the energy balance are presented in Appendix 3. The energy required to fix the carbon atoms in 1 mole of biomass was found to be 78,584,302 J. Energy consumed or released by the reactants and products as presented by the chemical equation 1 in the Materials and Method section was calculated to determine the net energy difference of the system. To compute energy of the reactants or product, standard molar enthalpies of each compound was determined and is presented in Appendix 3. The standard molar enthalpies of each compound were then multiplied with their respective mole numbers to determine the enthalpy of reactants and products. The net enthalpy of the reactants was found to be -23246.96 KJ and for the product it was found to be -27047.684 KJ. The net energy loss of the system was calculated by subtracting net enthalpy of reactants from net enthalpy of product which was found to be -3800.724 KJ. Since, the sum of the enthalpies of reactants is greater than sum of the enthalpies of the products, the net energy loss of the reaction is less than zero. This negative energy loss indicates that the reaction is exothermic and total of 3961.25 KJ of energy released to the surroundings.

4.2. Light Analysis

Light plays an important role in microalgae growth and biomass production and therefore, light analysis was performed using data from a previous study. A randomized block design test was performed to determine the significance of path length and flow rate on light intensity. The path length was considered as treatment and flow rate was considered as block. A total five treatments and 10 blocks were analyzed. The null hypothesis for the t-test assumed that all means are equal and the alternative hypothesis assumed that at least one mean is different. The F-statistics of the analysis was found 104.8 which was greater than tabulated F value of 2.59356 which indicates that the null hypothesis should be rejected. Thus, this result suggests that path length has a significant effect on light intensity. The summary of randomized block design test result is presented in Table 15 and detail analysis is present in Appendix 4.

Table 15. Output of randomized block design test

Source of variation	Degree of Freedom	Sum of Squares	Mean squares	F-Value
Treatments	4	3567.40	891.85	104.8
Blocks	9	1190.32	132.26	
Error	36	291.35	8.09	
Total	49			

Since, we reject the null hypothesis, Tukey-HSD multiple comparison analysis was performed to determine statistical difference between the treatments. The overall output of the Tukey's test is presented in Appendix 5. Table 16 presents the groups of the treatment. Letter a,b,c and d represents the different groups. It was found that the mean of light intensities at path length 102 mm and 152 mm had same group and therefore, the mean light intensity of both pathlengths are equal. While mean of light intensities for

path length of 203 mm, 254 mm and 305 mm had different groups and therefore, the mean light intensities are significantly different from each other. Thus, this indicates that the pathlengths 102 mm and 152 mm had similar effect on light intensity whereas effect of pathlengths 203 mm, 254 mm, and 305 mm on light intensity differ from each other.

Table 16. Groups of different path length

Pathlength (mm)	Light Intensity	Groups
102	66.854	a
152	64.247	a
203	55.398	b
254	49.993	c
305	44.397	d

Table 17. Groups of different flow rate

Flow rate (LPM)	Light Intensity	Groups
1	65.844	a
2	61.792	ab
3	59.778	abc
4	58.080	bc
5	56.002	bcd
6	53.814	cd
7	53.770	cd
8	51.678	d
9	51.066	d
10	49.954	d

Similarly, the Tukey HSD for flow rate was also performed and the summary of output is presented in Table 17. The calculation details and outputs are presented in Appendix 6. Result showed that there is no significant difference in the mean of the light intensity for flow rate 1, 2, and 3 and therefore, they are categorized as group “a”. Likewise, the mean

light intensity for flow rate 2, 3, 4, and 5 are same and are categorized as group “b”; flow rate 3,4,5, 6, and 7 are same and categorized as group “c”; and flow rate 5,6,7,8,9, and 10 are same and categorized as group ‘d”. This indicated that the flow rates in each group had similar effect on light intensity.

Also, linear regression analysis was performed to fit a model for light intensity, flow rate, and path length. For this analysis, light intensity was considered as the dependent variable whereas flow rate and path length were considered as the independent variables. Summary of model is presented in Appendix 7. The fitting model obtained is given in equation (16):

$$Light\ Intensity = 98.401 - 0.613 * Pathlength(mm) - 3.374 * Flowrate + 0.008 * (Flowrate * Pathlength) \quad (16)$$

The multiple R^2 of the above model was found to be 0.949 indicating a good fit of the residuals around the regression line. Also, p-value at 95% confidence level for path length, flow rate, and the interaction was found to be <2E-16,1.39E-12, and 4.69E-06 respectively, suggesting that path length, flow rate, and its interaction have a significant effect on light intensity. The residual plot for path length and flow rate is shown in Figure 22.

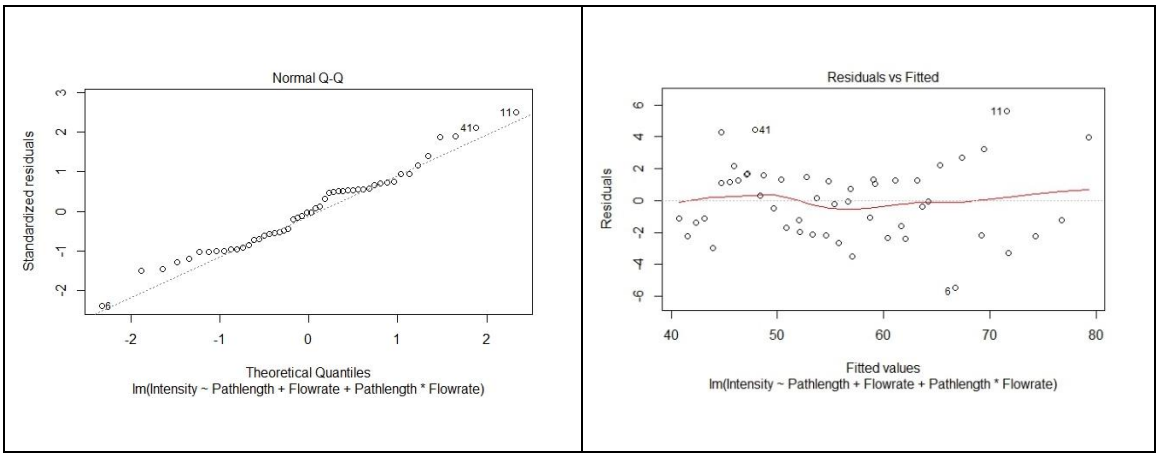

Figure 22. Path length residual plot and flowrate residual plot

In normal Q-Q plot, the residuals are closer to the fitted regression line indicating fitted values closer to the observed values and in the residuals versus fitted plot, the majority of the residuals are around the mean line. This result suggests that the relationship between the independent variables (flow rate and path length) and the dependent variable (light intensity) is linear.

4.3. Sparger Design

The diameter of the sparger used for the reactor with cross-sectional area 300 inch^2 (0.19 m^2) was found to be ½ inch (1.27 cm) using SPARGER software. The total gas discharge into the PBR by a sparger with a diameter of 1.27 cm was found to be 11.81 LPM (0.000197 m^3/sec), consisting of 5% CO_2 and 95% air mixture. Thus, the superficial gas velocity was found to be 0.0010 m/sec by dividing total gas discharge with cross sectional area of the reactor (Falinski, 2009). The velocity of the gas mixture before the first hole was determined as 1.56 m/sec and the Reynolds number was found to be 1960.342 indicating gas flow is laminar flow in the sparger. The type of gaseous flow in the reactor system is an important part of designing sparger. It is desired to have laminar

flow. In laminar flow, gas mixture moves with the same speed in same direction with minimum or no cross-over of gas streams. This allows minimum or no damage of algae cells resulting better growth of algae and high biomass production compared to high turbulence flow. Sparger causing high turbulence flow in the reactor may damage algae cells and reduces biomass production (Xiao et al., 2016). The hydraulic diameter of the rectangular PBR was found to be 0.85 ft (0.26 m) using equation developed by Kommareddy et al. (2013).

The values of superficial gas velocity (0.0010 m/sec) and hydraulic diameter (0.26 m) indicate that the flow falls into the homogenous bubble flow regime as suggest in the column diameter versus gas velocity plot (Figure 9). This result suggests that the designed sparger provides homogenous and uniform mixing of gases in the reactor.

The total number of holes in the sparger was calculated to be 30 at a hole spacing of 40.4 mm. Also, the software simulation result showed no weep condition for the designed sparger which means that the gas flow velocity in the sparger will be above the critical weep velocity. Weep condition in the sparger is not desired as it may cause flow of media into the sparger resulting poor bubble formation and irregular gas mixing in the system. The gas velocity profile that was obtained from the software is plotted in Figure 23. Hole velocity profile of a sparger. It was found that the hole velocities (exit velocities) were slightly declining from 21.44 m/sec to 20.5 m/sec along the length of sparger.

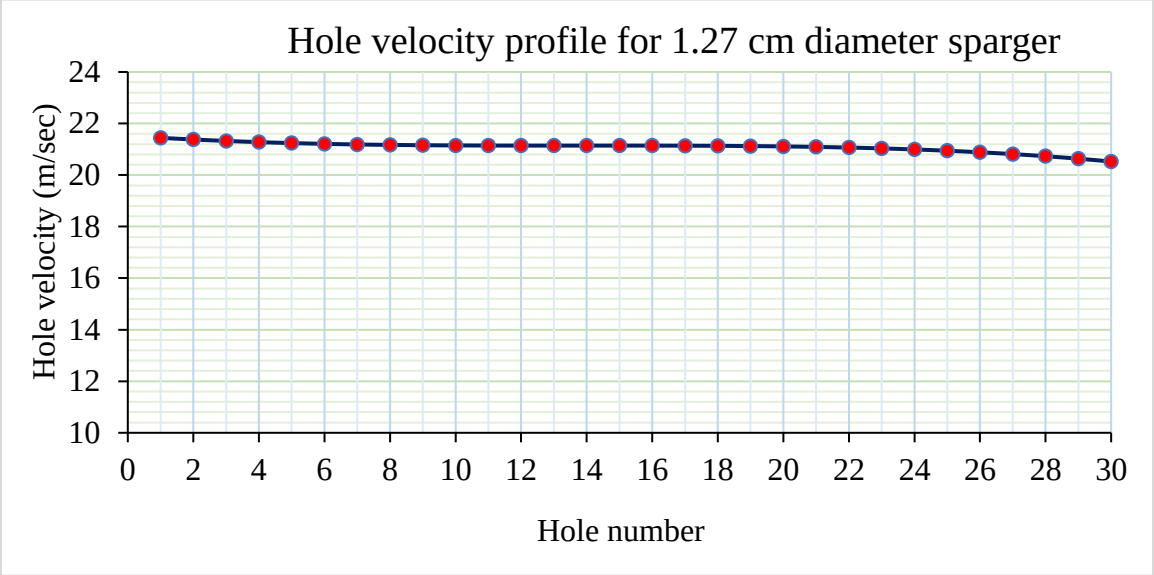

Figure 23. Hole velocity profile of a sparger

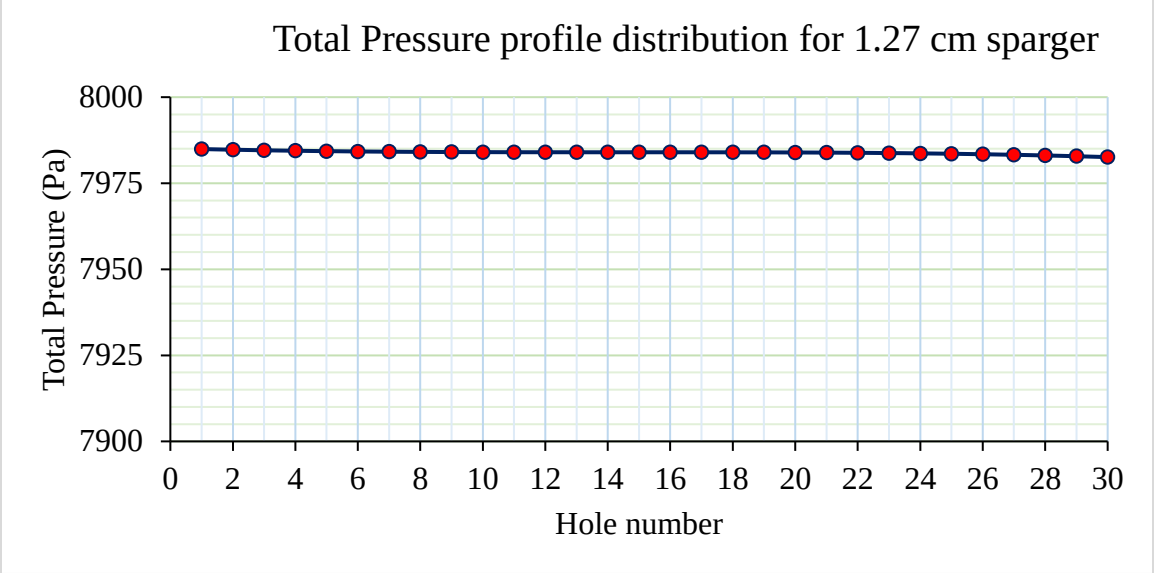

Figure 24. Pressure profile distribution along the length of sparger

The ENU was found to be 4.29% which means that 95.71% of the pressure was distributed uniformly along the length of the sparger. The pressure distribution profile plot is shown in Figure 24 and indicate that there is a slow decline along the length of the sparger from 7984.79 Pa to 7982.40 Pa. Increase in ENU impacts the pressure drop and

reduces the interfacial area (Kulkarni et al., 2007). The pressure distribution variation along the length of the sparger may lead to non-uniform mixing of gases in the PBR. This causes formation of dead zones (zones of low mixing) in the PBR due to inadequate gas mixing in the PBR. The formation of dead zones in the reactor indicates poor bubble distribution and mixing by the sparger. Therefore, it is important to check the uniformity of the pressure distribution of the designed sparger to avoid dead zone formation.

The Sparger software also simulated the percentage of air/gas remaining after the last hole in the sparger. It is very important that the designed sparger should equally distribute all the air/gas supplied to the sparger through each sparger hole and the percentage of air/gas remaining after the last hole should be equal to zero. The percentage of air/gas remaining after the last hole in the designed sparger was found to be nearly zero (0.68%). This result indicates that the mass balance for the sparger was achieved. The plot of hole air profile along the length of the sparger is shown in Figure 25. The sum of all the orifice air flow rates in the sparger resulted in total sparger discharge of 0.000196 m^3/s which was found almost equal to the total air flow rate of 0.000197 m^3/sec supplied to the sparger. The duct air flow along the length of the sparger was also calculated by the software and the plot is shown in Figure 26. The simulation result shows air flow rate in duct decreases linearly. This is due to decrease in air pressure in the duct along the length of the sparger. Since, the frictional loss increases along the length of the sparger, it causes decrease in air pressure which ultimately decreases flowrate in the ducts of the sparger.

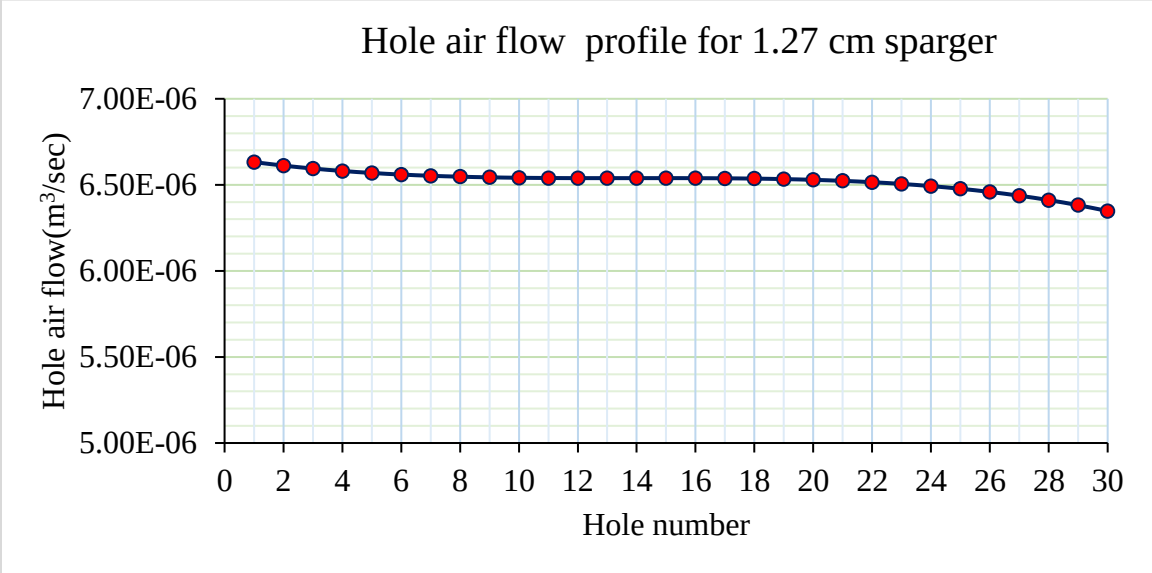

Figure 25. Hole air flow profile along the sparger

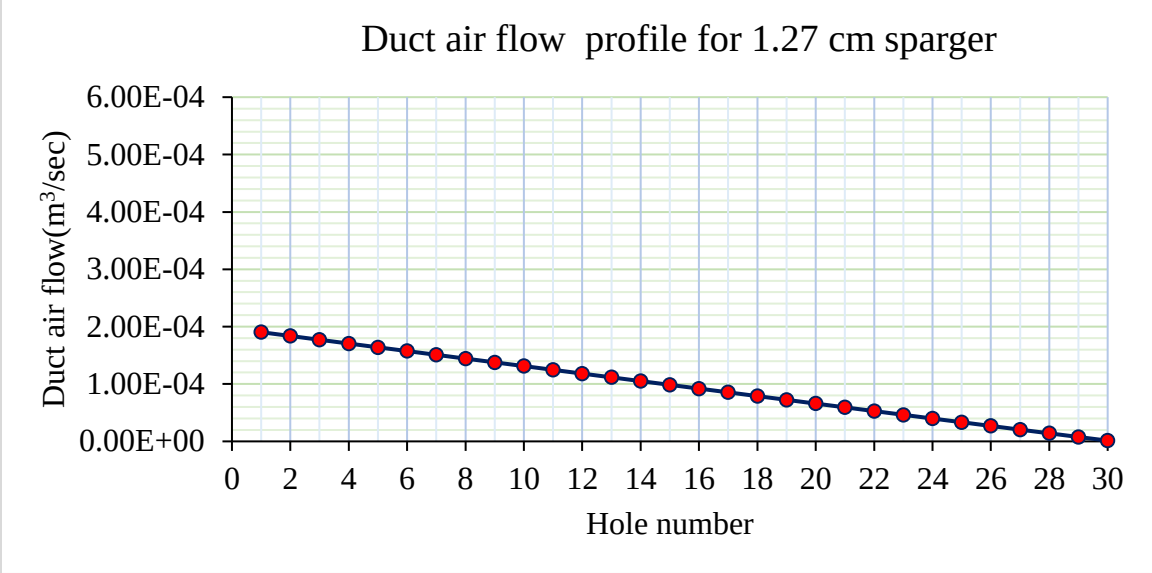

Figure 26. Duct air flow along the sparger

The bubble size distribution along the length of the sparger was also calculated. The average bubble diameter was found to be 3.94 mm to 3.92 mm along the length of the sparger. The mean of the bubbles diameter was found to be 3.93 mm with a very small deviation of 0.0027. Also, coefficient of variance was found to be 0.07% which

indicates that there is less variance in the mean of the bubbles diameter. The calculated value of bubble diameter showed homogenous flow in the reactor. The size of the bubbles plays an important role in the gas mixing and algae growth in the reactor. Small bubbles tend to block the light. Small bubbles have a greater surface area to volume ratio. Therefore, mass transfer coefficient (Kla) is higher. The large bubbles rise up very quickly and break faster when compared to small bubbles which leads to improper mixing of nutrients in the PBR and algae cell damage. The bubble size distribution from the holes of the sparger is plotted in Figure 27.

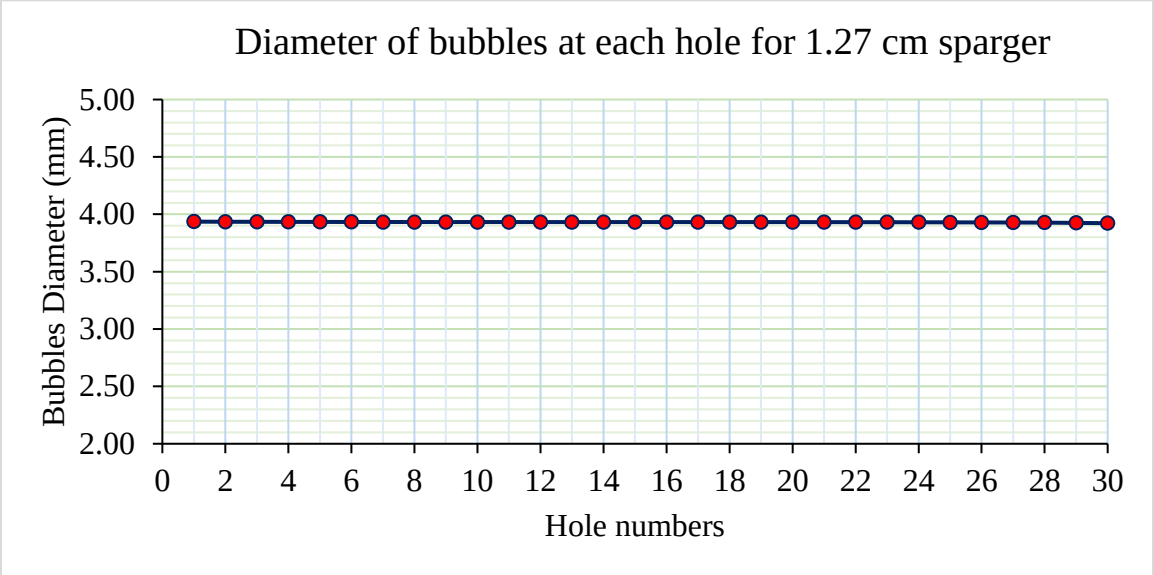

Figure 27. Estimated bubbles diameter along the hole of the sparger

4.4. Study of flow patterns

The analysis of air/gas flow patterns was performed to determine the uniformity of the bubble distribution and proper mixing of the supplied air/gas mixer in the media. This analysis was based on three different factors; number of sparger pipes, air/gas flow rate,

and depth of water in the reactor. Effect of each factor on the flow patterns are explained next:

4.4.1. Based on the different number of pipes

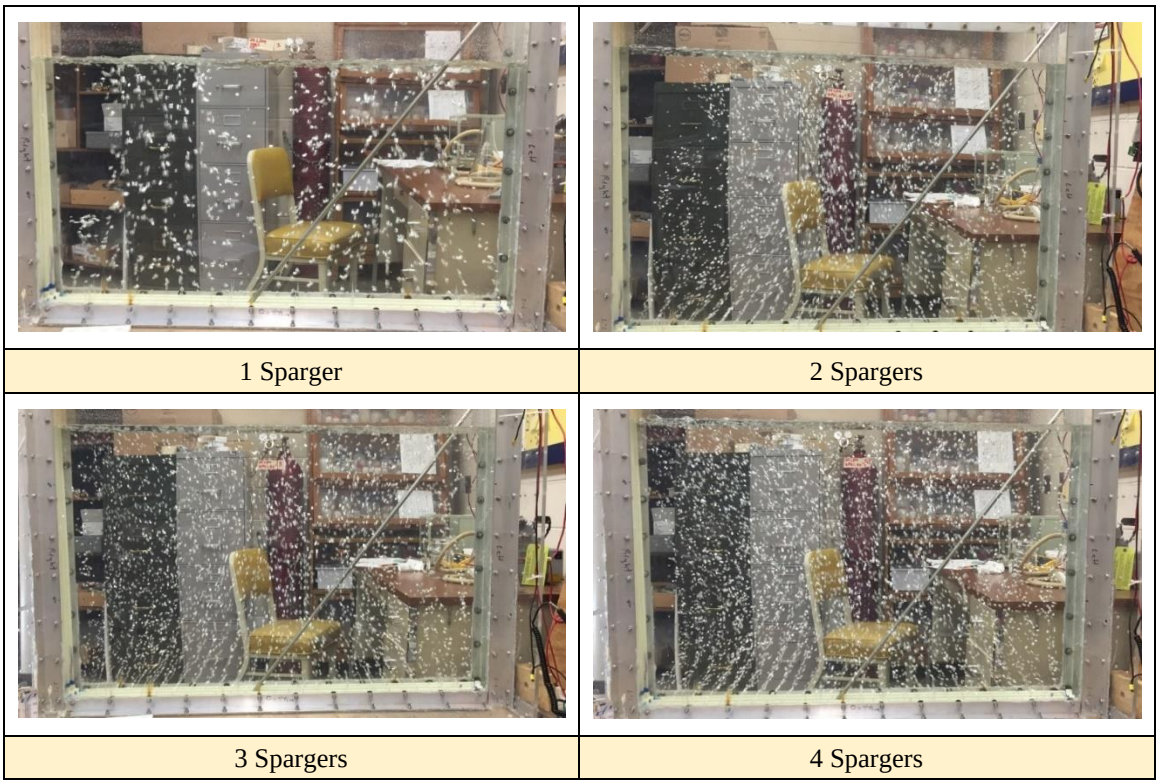

1 Sparger	2 Spargers
3 Spargers	4 Spargers

Figure 28. Flow patterns for 10 LPM (0.000167 m3/sec) at 30-inch (76.2 cm) water height for 1 to 4 spargers.

Figure 28 shows the flow pattern of the bubbles with 1, 2, 3, and 4 sparger pipes under a constant flow rate and water height. The reactor was first tested with single sparger pipe in the reactor. The mixing in the reactor was observed to be non-uniform with large bubbles. This suggested that the single sparger is not sufficient to provide uniform mixing and bubble distribution for the given reactor size. The sparger number was then increased to two and observation were made. The mixing and bubble formation was observed improved with 2 spargers compared to single sparger. However, this was also observed

insufficient for adequate mixing and bubble distribution. Also, the mixing was more on the middle of the PBR than on the end. Likewise, the number of spargers increased to 3 and 4. With 3 spargers, the mixing and bubble distribution was observed much better compared to single and double sparger systems. It was observed that the mixing was found from the end to the middle. The mixing was observed to be much improved when the reactor was run with 4 spargers. The size of bubbles observed was smaller and better distribution in the reactor. This analysis suggests that more spargers results in better bubble formation and mixing in the PBR. The gas coming out from the less number of sparger may not be sufficient to mix all the nutrients within the medium. Less number of sparger means the less number of bubbles and with the less number of bubbles all the medium in the PBR cannot be in suspension.

4.4.2. Based on different flow rate

Figure 29 shows the flow pattern of the bubbles for air flow rate of 10 LPM, 20 LPM, 30 LPM, and 40 LPM in the reactor with 4 number of spargers and 30-inch of water height. At the lowest flow rate of 10 LPM, bubble distribution was found to be uniform from all the orifices of the sparger. Also, the mixing of air was observed uniform and the flow pattern was found similar to that of a bubble column PBR. At 20 LPM the mixing was found to be more at the center which leads to poor mixing on the end side of the PBR. At higher flow rate, the mixing was observed uneven and flow pattern resembled to turbulent flow. Also, increasing the flow rate showed cluster formation of air bubbles in the middle of PBR causing circular movement of air bubbles. The increase in flow rate will increase in superficial gas velocity and this will result the bubbles diameter to be larger (Kaidi et al., 2012). This characteristic of air flow pattern under high flow rate was

observed similar to that of an airlift photobioreactor without any riser wall. However, the volume of the down comers seems to be not sufficient to mix the gas into the water at the bottom end and this may lead to poor mixing on that area. Thus, the results suggested optimum flow rate of 10 LPM for better bubble distribution and homogenous mixture of air for the reactor with water height 30-inch and 4 spargers.

10 LPM (0.000167 m^3/sec)

20 LPM (0.000333 m^3/sec)

30 LPM (0.0005m^3/sec)

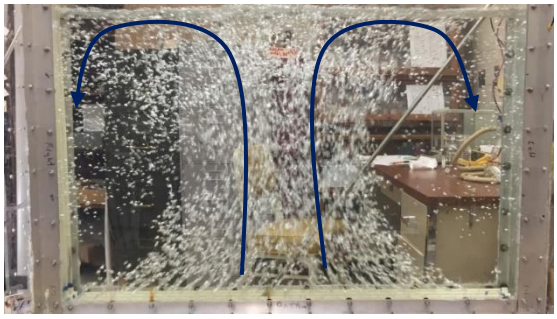

40 LPM (0.00067 m^3/sec)

Figure 29. Flow patterns for 4 number of spargers at 30-inch (76.2 cm) water height for 10, 20, 30, 40 LPM

4.4.3. Based on different height

Figure 30 shows the flow pattern of the bubbles in the PBR with water levels of 15-inch, 20-inch, 25-inch, and 30-inch under constant flow rate of 10 LPM, and 4 spargers. When the water height in the PBR was 15-inches, the bubbles were observed to be bigger in diameter but the distribution of bubbles were uniform in the reactor. The bubbles were

observed moving upward exhibiting similar pattern like in bubble column PBR with only one riser. Increasing water height above 20-inches resulted in smaller bubble formation with uniform distribution of the bubbles and air mixing in the reactor.

15-inch (38.1 cm) water height

20-inch (50.8 cm) water height

25-inch (63.5 cm) water height

30-inch (76.2 cm) water height

Figure 30. Flow patterns at 10 LMP (0.000167 m3/sec), 4 spargers, and water height of 15, 20,25, and 30-inch

This analysis suggests that with the change in the depth of the water there is change in the flow patterns. With the increase in the height (30-inch) the flow pattern at the end of the sparger was different than the middle of the PBR. The bubbles flow vertically upward in the middle of the PBR whereas at the end of the spargers the bubbles flow exhibits the similar behavior to that of the air lift reactor with riser and down comer. It may have occurred because with the reduced in depth of water there may be little air flow along the length of the sparger.

It was found that sparger pipes should be straight at the bottom of PBR. It was observed that small change or deformation in sparger pipe greatly affects the air flow regime and distribution uniformity. A well leveled sparger pipe allows uniform formation of bubbles and upward mixing in the reactor. This is mainly caused by uniform pressure distribution at each sparger holes (orifice) along the length of the sparger. However, if there is any distortion along the length of the sparger pipe, bubble formation mostly occurs though the holes which are at relatively flatter position and the mixing of air bubbles follows either spherical shape or elliptical shape. This mostly happens when the lower depth of water was over sparger.

4.5. Biomass growth and physical parameters

4.5.1. Biomass Growth

Figure 31 shows a graph of the average biomass concentration from Day 0 to Day 16. The initial concentration of the algal biomass was 10 mg/L on day 0. An increasing trend was observed in the biomass as the number of algal cells were multiplied expeditiously. The algal biomass weight was measured in every 12 hours and a daily average weight was calculated. The lag phase was observed in the first 24 hour. It may have occurred because microalgae take some times to adapt the new environment condition (Rolfe et al., 2012). From day 2 to day 3, rapid growth was observed and the biomass increased up to 24 times the initial.

Overall slow growth was observed from day 3 to day 11. At the end of the day 7 biomass again dropped to 426 mg/L and the stagnant growth was observed until day 11. Declining in carbon to nitrogen ration may be the reason of the stagnant growth rate (Mahapatra et

al., 2013). The highest biomass weight was recorded to be 928 mg/L on day 13. The biomass weight starts to drop rapidly after day 13 as the media in the reactor become insufficient to provide adequate nutrient for further algal growth. Among all the nutrients provided in BG11, phosphorous is the one that will be depleted soon compared to other nutrients by the cyanobacteria (Vijayakumar, 2015). Removing some medium from PBR and adding the fresh medium may help in regrowth of cyanobacteria and take the peak after some days (Anderson et al., 2016).

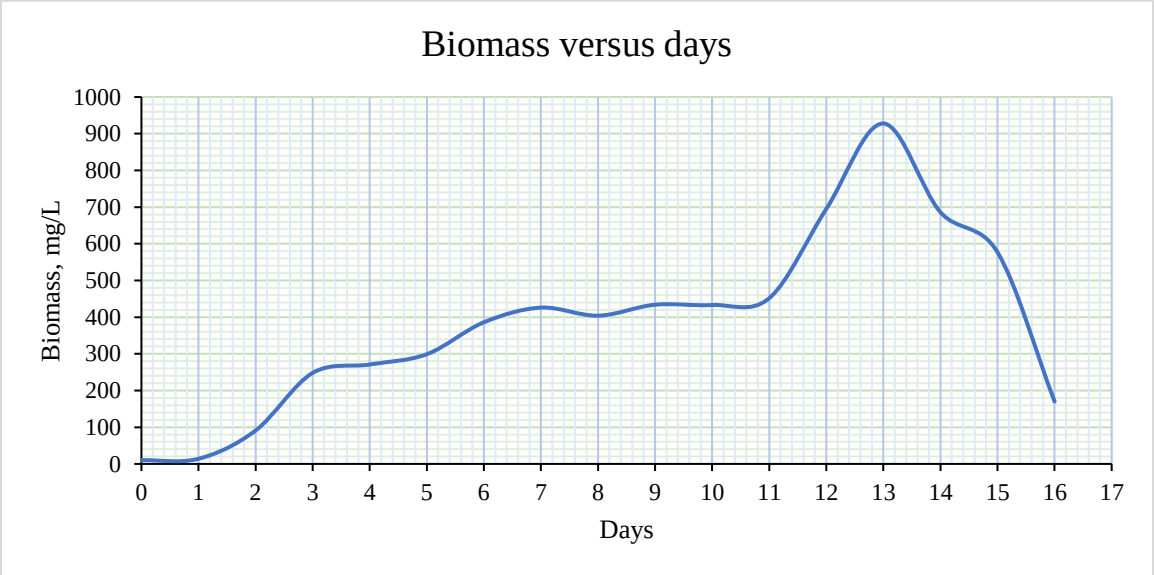

Figure 31. Biomass growth rate curve for 132L PBR

4.5.2. Physical parameters ORP, DO, pH and temperature

Figure 32 shows the variation in the physical parameters of the growth medium during the experimentation period. The decrease in ORP nominally follows the cyanobacteria growth. This decline in the ORP suggest that consumption of the nutrients by the algal biomass in the reactor. When the concentration of algal biomass was less in the medium in the beginning, the nutrient (ions) consumption rate was also less and therefore, the

value of ORP was higher (327.67 mV on day 1) which means that it has higher oxidizing agent. When there was rapid growth of biomass in day 2 and day 3, the ORP value decreased. A slower decrease in ORP was found from day 3 to 11 when there was slow growth in biomass concentration. Similarly, the ORP was found to be decreased when the biomass was at peak on day 13. Now, as the algal biomass concentration started to decrease in the reactor on day 16, the ORP value also decreased. It was observed that the overall trend of ORP is decreasing in phase from the start to the end. It indicates that the more nutrients were consumed which causes decrease in ORP (69.76 mV) until the last day. Nutrients are being consumed faster than being produced. The positive value of ORP indicates that the medium has oxidizing agent.

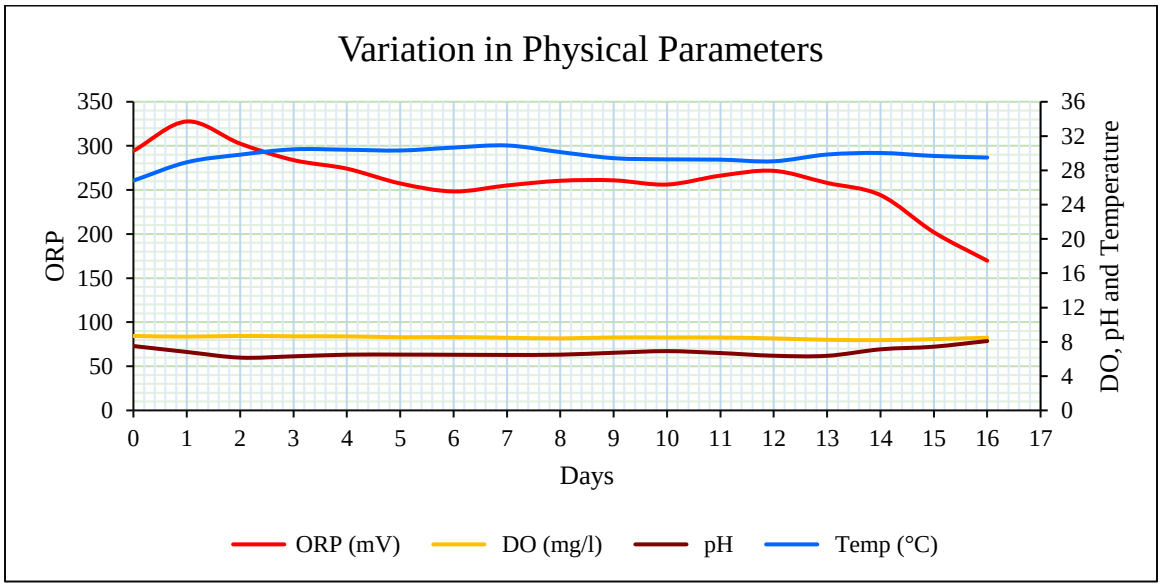

Figure 32. Variation in physical parameters of the growth medium

A small variation was observed in the DO throughout the experimentation period as there was continuous supply of the air to the reactor. This indicates that the there is no buildup of O_2 from the photosynthesis O_2 removal process. The temperature that was maintained

in the PBR during the experiment was in the range of 26.81°C and 30.91°C. The temperature was low for the first day then it increased from second day. This may be because it took 24 hours to absorb the heat from the light by the medium. After then the temperature of the medium was maintained almost constant throughout the experimentation period. The constant room temperature and continuous light supply from the LED panels provided the heat to the medium, thereby helping to maintain uniform temperature. This temperature is suitable for this species growth.

The initial pH of the medium was recorded 7.51. For the first 24 hours when only air was sparged into the reactor so that the transferred culture would not get a shock from a new environment. After 24 hours, CO_2 was supplied which lowers the pH of the medium. When there was a rapid growth in the biomass there was a drop in pH from day 0 to day 3. Similarly, from day 3 to 11 there was a small variation in pH with a slower growth in biomass. Again, when there was rapid increase in biomass on day 11 to day 13, decrease in pH was observed. Finally, when the biomass was rapidly decreasing the pH was observed to be increased rapidly. The inverse relationship was observed between the pH and the ORP throughout the experiment. It is because the pH measures the hydronium ion present in the medium where as ORP measures the total ions present in the medium. Increase in ORP is due to the H^+ ion from the increase in CO_2

Also, it was found that the CO_2 has direct impact on pH. An increase in CO_2 flow rate resulted in a decrease in the pH and vice versa. The plot of CO_2 flow rate versus pH is as shown in Figure 33.

The pH was found maximum on Day 0 with value of 7.5 and when CO_2 supply to the medium was increased to 124.5 ml/min on day 2, the pH was dropped to 6.15. Since, the

pH was dropped drastically, the CO_2 supply was reduced to 93.76 ml/min on day 3. When the CO_2 was gradually decreased to 62.03 ml/min, pH gradually increased to 6.51 on day 4 and 5. Similarly, throughout the experiment the CO_2 was varied to balance the pH. If the CO_2 intake was higher than the pH value will decreased which will make the medium more acidic. When the CO_2 was lower, pH will rise but care should be taken that the proportion of CO_2 should not be less than 0.2% compared to air because the medium will not have the sufficient source of carbon for photosynthesis. The data of biomass and its physical parameters are presented in Appendix 8.

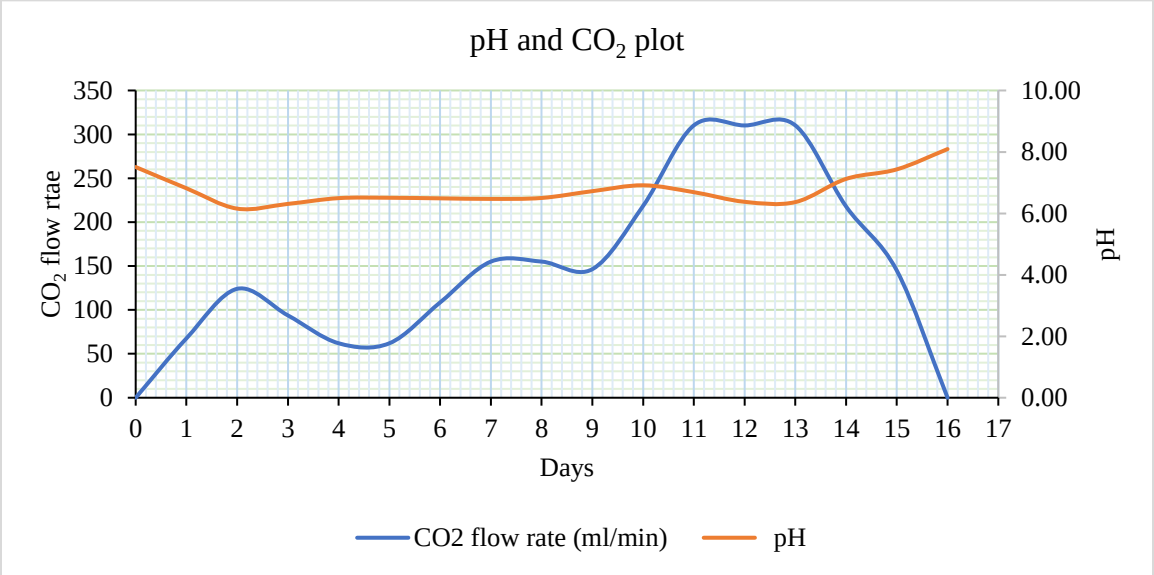

Figure 33. Graph of pH and CO_2 flow ate

Statistical Analysis

Multiple linear regressions were performed to determine the relationship between algal biomass and physical parameters. The algal biomass was considered as the dependent variable and physical parameters (DO, ORP, pH, and temperature) were considered to be the independent variables. The p-value at 95% confidence level showed that all the

physical parameters have a significant effect on algal biomass. Among all the physical parameters, pH and DO was found to have most significant effect on algal biomass with p-value of 1.88e-06 and 3.75e-05. The regression equation obtained is shown in equation (17) –

$$Biomass\ \left(\frac{mg}{L}\right) = 18844.90 - 3.63 * ORP(mV) - 1377.04 * DO(\frac{mg}{L}) - 403.26 * pH - 104.32 * Temperature(°C) \quad (17)$$

The multiple R-squared of the above model was found to be 0.927 and adjusted r-squared was found to be 0.903. This regression model accounts about 93% of the variance which indicates that the data points are very close to the fitted regression line. Also, higher R-squared value indicate a better model fit suggesting that each physical parameter greatly affects the algal biomass production. The overall regression model output is provided in Appendix 9 and the normal Q-Q plot and residuals versus fitted plots are shown in Figure 34.

In normal Q-Q plot, the residuals are closer to the fitted regression line indicating fitted values closer to the observed values and in the residuals versus fitted plot the majority of the residuals are around the mean line. Thus, multiple linear regression analysis result suggests that DO, ORP, pH, and temperature play significant roles in algal biomass production under a controlled environment.

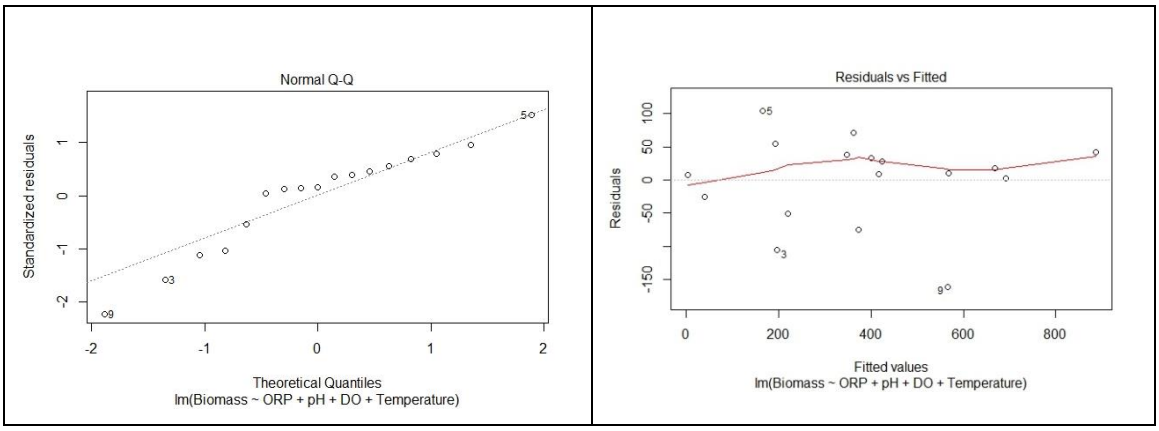

Figure 34. Normal Q-Q plot and residual vs fitted plot

4.5.3. Biomass and gas flow rate

Figure 35 shows the plot of algal biomass versus gas flow rate throughout the experimentation period. For a bigger PBR, constant flow rate is considered insufficient for adequate mixing and preventing the algal biomass from settling. Since the algal biomass increases with time, the flow rate also needs to be increased to keep the algal biomass suspended in the medium and provides proper air/gas mixing. If a constant flow rate is maintained, it will become inadequate to keep the increasing biomass concentration suspended which will result in biomass settling to the bottom of the reactor. Thus, the flow rate adjusted regulated throughout the experimentation period with increasing biomass concentration to maintain uniform mixing and avoid biomass settling. The CO_2 flow rate was changed based on pH of the medium. Data of flow rate and biomass of each day is present in Appendix 10.

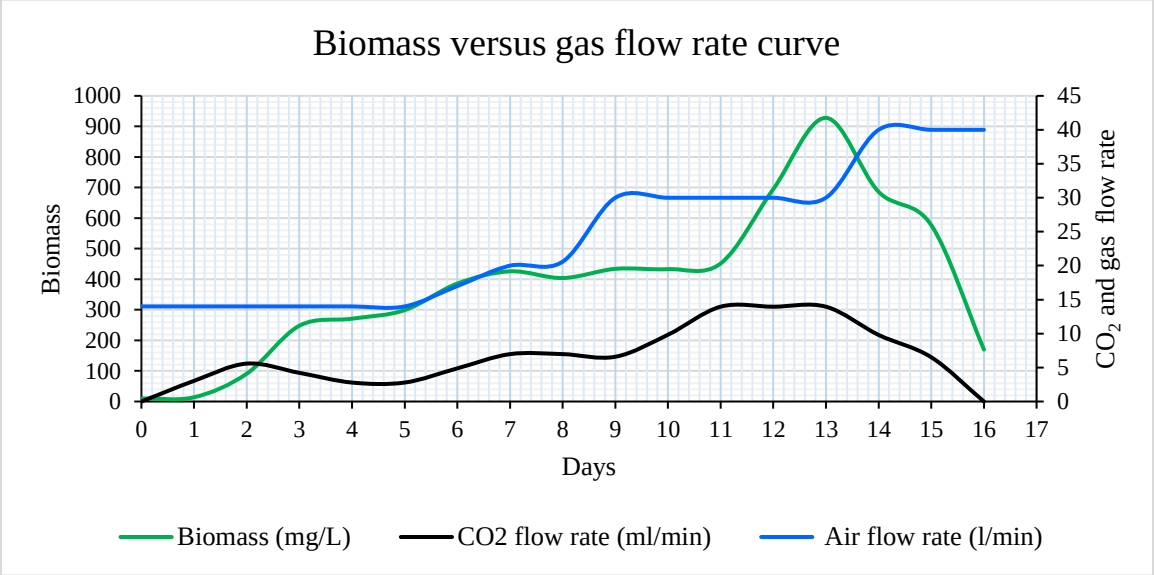

Figure 35. Biomass and gas flow rate plot.

Statistical Analysis

Multiple linear regressions were performed to determine the impact of flow rate (air and CO_2) on biomass. The algal biomass was considered as dependent variable and CO_2, and air flow was considered as the independent variables. The p-value at 95% confidence level showed that CO_2 flow rate has a significant effect on algal biomass concentration (growth) with a p-value of 0.000492 (<0.05). The p value of air flow rate (0.0639) at 95% confidence level showed that air flow rate has no significant effect on biomass growth. This analysis does not show the impact of air flow rate on biomass growth. However, the air flow rate showed a direct impact on the biomass settling during experiment. It may have been occurring because of less number of data. The regression model obtained is given as equation (18) –

$$Biomass\ \left(\frac{mg}{L}\right) = 1.694 * CO2\ flow\ rate\ \left(\frac{L}{min}\right) - 45.194 \quad (18)$$

The multiple R^2 for the above model was found to be 0.74 and the adjusted R^2 was found to be 0.703. This regression model accounts about 74% of the variance which indicates that the data points are close to the fitted regression line. Also, R-square indicates a good model fit suggesting that each CO_2 flow rate positively affects the algal biomass production. However, multiple R^2 value of gas flow rate (0.74) is not good compare to multiple R^2 of the physical parameters (0.93). This shows that the physical parameters data points are closer to the fitted regression line than the flow rate. The overall regression model output is provided in Appendix 11 and the normal Q-Q plot and residuals versus fitted plots are shown in Figure 36.

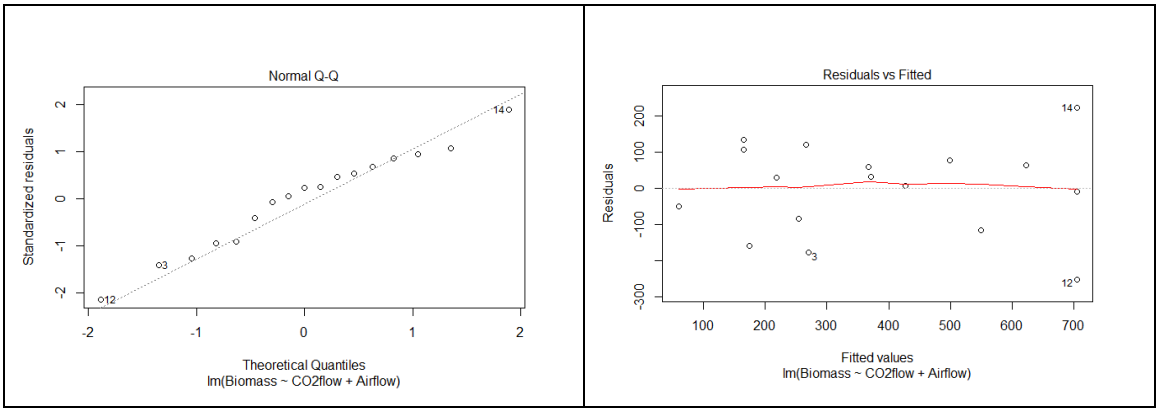

Figure 36. Normal Q-Q plot and residual vs fitted plot

In normal Q-Q plot, the residuals are closer to the fitted regression line indicating the fitted values are closer to the observed values and in residuals versus fitted plot, majority of the residuals are around the mean line. Thus, multiple linear regression analysis results suggest that the CO_2 flow rate has significant effect on algal biomass production under controlled environment.

4.5.4. Comparison of 132L PBR with 13L flat plate PBR

The comparison of biomass concentration of 13L and 132L reactor was made using previous data and current research data. The biomass concentration versus days was plotted for 13L reactor and 132L PBR as shown in Figure 37. The maximum concentration of biomass was found to be 960 mg/L and 928 mg/L for 13 L and 132 L PBR, respectively. This observation indicates that the both the reactors have similar algal biomass production. However, the maximum algal biomass in 13L PBR was achieved on 19th day of experiment whereas in 132L PBR, the maximum algal biomass was achieved in only 16 days. This suggests the PBR size does have some degree of effect on algal biomass production time.

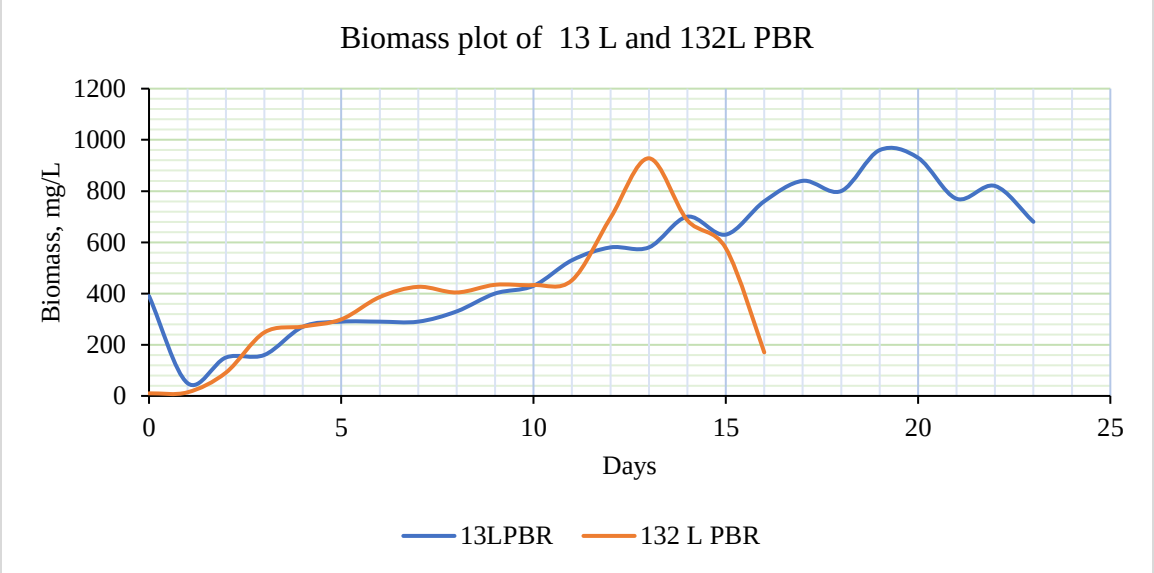

Figure 37. Comparison of biomass of 13L and 132L reactor

Similarly, air and the CO_2 flow rate (1LPM air and 50ml/min CO_2) was kept constant and biomass was in suspension throughout the experiment in 13L PBR. But in the 132L PBR

the flow rate was varied to keep the biomass in suspension. This may be the reason that the biomass concentration was achieved higher in 132L reactor.

Likewise, comparison of physical parameters (pH, DO, ORP, and temperature) for both the reactors were analyzed. The plot of pH, DO, ORP, and temperature for both the reactors is presented in Figure 38. There is a drop in pH in 132 L reactor in the beginning because the CO_2 was not supplied until day 1 and this also leads to increase in ORP. Also, there is drop in pH on day 11 to 13 because of the variation of the CO_2 supply. The plots for all the physical parameters showed a similar trend.

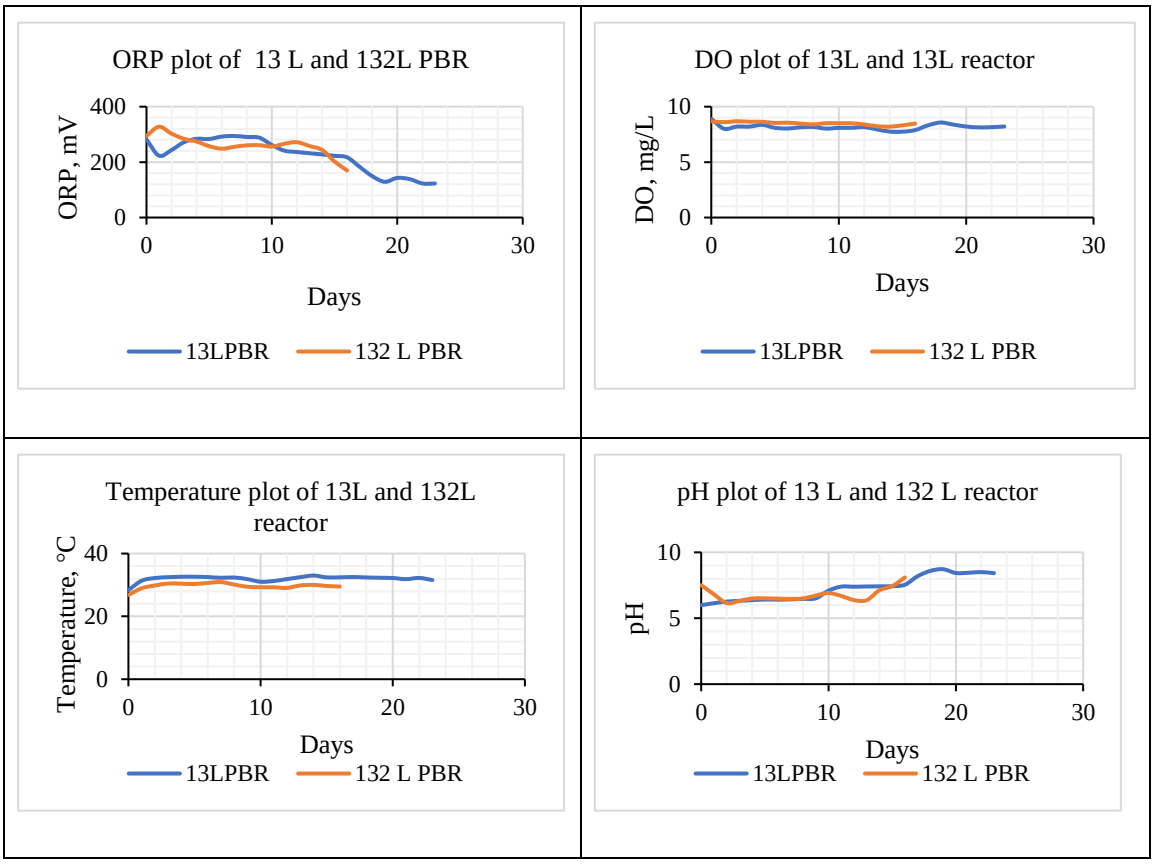

Figure 38. Plot of physical parameters for 13 L and 132L PBR.

Statistical Analysis

Statistical comparison of algal biomass production of both the reactor was performed using student's t-test assuming two samples with unequal variance. The null hypothesis set was the 13L reactor biomass and 132L reactor biomass means are equal and the alternate hypothesis was 13L reactor biomass means is not equal to the 132L reactor biomass. The value of t-statistics was found 1.764 which was smaller than t-critical (i.e. 2.028) at 95% confidence level and therefore, the null hypothesis was found true. The analysis result is present in Table 18.

Table 18. Student's t-test: two sample assuming unequal variances

	Biomass (13L)	*Biomass (132L)*
Mean	526.25	383.7411765
Variance	70137.5	61228.66382
Observations	24	17
Hypothesized Mean Difference	0	
df	36	
t Stat	1.76433907	
P(T<=t) one-tail	0.043079662	
t Critical one-tail	1.688297714	
P(T<=t) two-tail	0.086159324	
t Critical two-tail	2.028094001	

This statistical comparison of two biomass means was found statistically insignificant indicating that the there is no difference in the biomass production between the 13L reactor and 132L reactor.

5. CONCLUSION

The major nutrients required for 1 g algal biomass production are Nitrogen (N), Phosphorous (P), Sulphur (S), Carbon (C), Magnesium (M), and Sodium (Na) and were found to be 0.09891g, 0.0256g, 0.0089g, 0.4925g, 0.0067g, and 0.16g respectively. Also, the overall energy loss from the reactions was found to be 3800.274 KJ and the system offers the exothermic reaction. However, the energy loss from the sparger air and the evaporation loss needs to be determined to find the total energy losses.

The linear equation was developed between the light intensity and the path length and flow rate. The developed equation will allow to find the value of light intensities at air flow rates from 1 to 10 LPM and the path length from 102 to 305 mm when used with red LED lights.

The ½ inch diameter sparger was designed using the SPARGER software. The simulated results met important parameters of the design consideration. The designed sparger met the low extent non-uniformity with the value of 4.29% and there was no weeping. The estimated bubble diameters ranged from 3.84 mm to 4.95 mm. The designed sparger was used for studying the flow patterns. Performance of the sparger at different flow rate, height and number of spargers pipe were evaluated.

Bubble diameter seems to be increased with the increase in flow rate and the reduced height of the liquid when operated at the same pressure. The number of sparger pipes in a PBR plays a big role in its performance. The increase in number of sparger pipes gives the better mixing then with fewer number of sparger pipe. Few sparger pipes may not have sufficient gas flow to mix all the nutrients within the medium. Fewer number of

spargers means the few number of bubbles and with the less number of bubbles all the medium in the PBR cannot be mixed. With the increase in flow rate and height, the mixing flow patterns look like the air lift reactor.

To reduce the sedimentation of biomass flow rate has to be increased with the increase in biomass. The sparger location plays a vital role in establishing different flow patterns. The sparger was located parallel to the reactor length and the riser was going upward in the reactor which when reached at the top then it radially bends to the width of the PBR. This indicates that the amount of air flowing in the PBR and the height of the medium will impact on the fluid flow patterns and the distance of the riser and the down comer.

Cyanobacteria did survive for 16 days in 132L medium flat plate photobioreactor using the design sparger for mixing. This reactor could produce 928 mg/L on the 13^{th} day of the experiment with the limiting nutrients. After the 16 days of experiment, the cyanobacteria was in declining phase because of consumption of nutrients supplied and CO_2 supply cut off.

The linear equation was developed between the biomass concentration and the CO_2 concentration. Also, the linear equation was developed between the cyanobacterial biomass concentration and the physical parameters (OPR, DO, Temperature and DO)

Biomass comparison and the physical parameters of 132 L flat plat PBR shows the similar trend to the 13 L flat plate PBR. This shows that the scaling up of the PBR has been successful but still there are lot of space for the research and experiment to make it better in the coming days.

6. FUTUREWORK

- PBR will be operated using the sparger in different orientation. The sparger pipe will be placed parallel to the breadth of the PBR and see if its impact on the flow patterns and growth of cyanobacteria is similar to the sparger placed parallel to the length of the PBR.
- Larger number of sparger holes will be simulated and check the performance of the PBR.
- The evaporation loss and the sparger loss for the 132L PBR will be performed to check the overall losses of the reactor.

REFERENCES

Abdo, S. M., E. Ahmed, S. A. El-Enin, R. S. El Din, and G. E. D. a. G. Ali. 2014. Qualitative and quantitative determination of lipid content in microalgae for biofuel production. *Journal of Algal Biomass Utilization* 5(3):23-28.

Ahmad, A. L., N. H. M. Yasin, C. J. C. Derek, and J. K. Lim. 2011. Microalgae as a sustainable energy source for biodiesel production: A review. *Renewable and Sustainable Energy Reviews* 15(1):584-593.

Al-Qasmi, M., N. Raut, S. Talebi, S. Al-Rajhi, and T. Al-Barwani. 2012. A review of effect of light on microalgae growth. In *Proceedings of the world congress on engineering.* London, U.K.

Alfano, O. M., R. L. Romero, and A. E. Cassano. 1986. Radiation field modelling in photoreactors—I. Homogeneous media. *Chemical Engineering Science* 41(3):421-444.

Anderson, G. A., S. Katuwal, A. Kommareddy, and S. Gent. 2016. Operation of a porous membrane photobioreactor. In *ASME 2016 10th International Conference on Energy Sustainability collocated with ASME 2016 Power Conference and the ASME 2016 14th International Conference on Fuel Cell Science, Engineering and Technology*. American Society of Mechanical Engineers.

Anderson, G. A., A. Kommareddy, T. Suess, and S. P. Gent. 2014. Review of Flow Patterns in a Column Reactor for Photobioreactor Application. In *ASME 2014 8th International Conference on Energy Sustainability collocated with the ASME 2014 12th International Conference on Fuel Cell Science, Engineering and Technology*. American Society of Mechanical Engineers.

Asmare, A. M., B. A. Demessie, and G. S. Murthy. 2013. Theoretical estimation the potential of algal biomass for biofuel production and carbon sequestration in Ethiopia. *International Journal of Renewable Energy Research* 3(3):560-570.

Barbosa, M. J., M. Janssen, N. Ham, J. Tramper, and R. H. Wijffels. 2003. Microalgae cultivation in air-lift reactors: modeling biomass yield and growth rate as a function of mixing frequency. *Biotechnology and bioengineering* 82(2):170-179.

Becker, E. W. 1994. *Microalgae: biotechnology and microbiology*. Cambridge University Press.

Benemann, J. R., and W. J. Oswald. 1996. Systems and economic analysis of microalgae ponds for conversion of CO{sub 2} to biomass. Final report.

Berberoglu, H., J. Yin, and L. Pilon. 2007a. Light transfer in bubble sparged photobioreactors for H2 production and CO2 mitigation. *International Journal of Hydrogen Energy* 32(13):2273-2285.

Berberoglu, H., J. Yin, and L. Pilon. 2007b. Light transfer in bubble sparged photobioreactors for H 2 production and CO 2 mitigation. *International Journal of Hydrogen Energy* 32(13):2273-2285.

Bilanovic, D., G. Shelef, and A. Sukenik. 1988. Flocculation of microalgae with cationic polymers—effects of medium salinity. *Biomass* 17(1):65-76.

Borowitzka, M. A. 1999. Commercial production of microalgae: ponds, tanks, tubes and fermenters. *Journal of biotechnology* 70(1):313-321.

Brar, A., M. Kumar, V. Vivekanand, and N. Pareek. 2017. Photoautotrophic microorganisms and bioremediation of industrial effluents: current status and future prospects. *3 Biotech* 7(1):18.

Brennan, L., and P. Owende. 2010. Biofuels from microalgae—A review of technologies for production, processing, and extractions of biofuels and co-products. *Renewable and Sustainable Energy Reviews* 14(2):557-577.

Burgess, G., J. G. Fernandez-Velasio, and K. Lovegrove. 2007. Materials, Geometry, Net Energy Ratio of Tubular Photobioreactor for Microalgal Hydrogen Production. *Int. J. Hydrogen Energy* 32(9):1225-1234.

Camacho, F. G., E. M. Grima, A. S. Mirón, V. G. Pascual, and Y. Chisti. 2001. Carboxymethyl cellulose protects algal cells against hydrodynamic stress. *Enzyme and microbial technology* 29(10):602-610.

Cañedo, J. C. G., and G. L. L. Lizárraga. 2016. Considerations for Photobioreactor Design and Operation for Mass Cultivation of Microalgae. In *Algae-Organisms for Imminent Biotechnology*. InTech.

Carvalho, A. P., L. A. Meireles, and F. X. Malcata. 2006. Microalgal reactors: a review of enclosed system designs and performances. *Biotechnology progress* 22(6):1490-1506.

Carvalho, A. P., S. O. Silva, J. M. Baptista, and F. X. Malcata. 2011. Light requirements in microalgal photobioreactors: an overview of biophotonic aspects. *Applied Microbiology and Biotechnology* 89(5):1275-1288.

Chen, C.-Y., J.-S. Chang, H.-Y. Chang, T.-Y. Chen, J.-H. Wu, and W.-L. Lee. 2013. Enhancing microalgal oil/lipid production from Chlorella sorokiniana CY1 using deep-sea water supplemented cultivation medium. *Biochemical Engineering Journal* 77:74-81.

Chen, C.-Y., K.-L. Yeh, R. Aisyah, D.-J. Lee, and J.-S. Chang. 2011. Cultivation, photobioreactor design and harvesting of microalgae for biodiesel production: A critical review. *Bioresource technology* 102(1):71-81.

Chen, F., Z. Liu, D. Li, C. Liu, P. Zheng, and S. Chen. 2012. Using ammonia for algae harvesting and as nutrient in subsequent cultures. *Bioresource technology* 121:298-303.

Chisti, Y. 2007. Biodiesel from microalgae. *Biotechnology Advances* 25(3):294-306.

Chisti, Y. 2008. Biodiesel from microalgae beats bioethanol. *Trends in biotechnology* 26(3):126-131.

Chisti, Y. 2013. Constraints to commercialization of algal fuels. *J Biotechnol* 167(3):201-214.

Christenson, L., and R. Sims. 2011. Production and harvesting of microalgae for wastewater treatment, biofuels, and bioproducts. *Biotechnology Advances* 29(6):686-702.

Davis, R., A. Aden, and P. T. Pienkos. 2011. Techno-economic analysis of autotrophic microalgae for fuel production. *Applied Energy* 88(10):3524-3531.

Dayan, C., A. Kumudha, R. Sarada, and G. A. Ravishankar. 2010. Isolation, characterization and outdoor cultivation of green microalgae Botryococcus sp. *Scientific Research and Essays* 5(17):2497-2505.

De Wilde, D., T. Dreher, C. Zahnow, U. Husemann, G. Greller, T. Adams, and C. Fenge. 2014. Superior Scalability of Single-Use Bioreactors. *Innovations in Cell Culture*:14.

Del Río, E., A. Armendáriz, E. García-Gómez, M. García-González, and M. G. Guerrero. 2015. Continuous culture methodology for the screening of microalgae for oil. *Journal of biotechnology* 195:103-107.

Demirbas, A., and M. F. Demirbas. 2010. *Algae energy: algae as a new source of biodiesel*. Springer Science & Business Media.

Dutta, K., A. Daverey, and J.-G. Lin. 2014. Evolution retrospective for alternative fuels: First to fourth generation. *Renewable Energy* 69(Supplement C):114-122.

Ebeling, J. M., P. L. Sibrell, S. R. Ogden, and S. T. Summerfelt. 2003. Evaluation of chemical coagulation–flocculation aids for the removal of suspended solids and phosphorus from intensive recirculating aquaculture effluent discharge. *Aquacultural Engineering* 29(1):23-42.

EIA. 2015. U.S. Crude Oil and Natural Gas Proved Reserves, Year-end 2015. U.S. Energy Information Administration.

EIA. 2017. Monthly Energy Review (MER). United States Energy Information Administration.

Energy Information, A. 2012. *Annual Energy Review 2011*. Government Printing Office.

Falinski, K. A. 2009. Effects Of Different Aeration Conditions On Isochrysis Galbana (T-Iso) Ccmp 1324 In A Bench-Scale Photobioreactor.

Finley, M. 2013. BP statistical review of world energy.

Fitzgerald, T. 2012. Frackonomics: some economics of hydraulic fracturing. *Case W. Res. L. Rev.* 63:1337.

Goldman, J. 1979. Outdoor algal mass cultures—II. Photosynthetic yield limitations. *Water Research* 13(2):119-136.

Griffiths, M. J., R. G. Dicks, C. Richardson, and S. T. L. Harrison. 2011. Advantages and challenges of microalgae as a source of oil for biodiesel. In *Biodiesel-Feedstocks and Processing Technologies*. InTech.

Grima, E. M., E. H. Belarbi, F. G. A. Fernández, A. R. Medina, and Y. Chisti. 2003. Recovery of microalgal biomass and metabolites: process options and economics. *Biotechnology Advances* 20(7):491-515.

Grobbelaar, J. U. 2010. Microalgal biomass production: challenges and realities. *Photosynthesis research* 106(1-2):135-144.

Hislop, D., and D. O. Hall. 1996. Biomass resources for gasification power plant. *Energy For Sustainable Development Ltd., University of London*.

Höök, M., and X. Tang. 2013. Depletion of fossil fuels and anthropogenic climate change—A review. *Energy Policy* 52:797-809.

Huang, J., J. Ying, F. Fan, Q. Yang, J. Wang, and Y. Li. 2016. Development of a novel multi-column airlift photobioreactor with easy scalability by means of computational fluid dynamics simulations and experiments. *Bioresource technology* 222:399-407.

Huang, Q., F. Jiang, L. Wang, and C. Yang. 2017. Design of Photobioreactors for Mass Cultivation of Photosynthetic Organisms. *Engineering* 3(3):318-329.

Hundt, K., and B. V. Reddy. 2011. Algal biodiesel production from power plant exhaust and its potential to replace petrodiesel and reduce greenhouse gas emissions. *International Journal of Low-Carbon Technologies* 6(4):294-298.

Hyndman, C. L., F. Larachi, and C. Guy. 1997. Understanding gas-phase hydrodynamics in bubble columns: a convective model based on kinetic theory. *Chemical Engineering Science* 52(1):63-77.

Jiménez, C., B. R. Cossío, D. Labella, and F. X. Niell. 2003. The feasibility of industrial production of Spirulina (Arthrospira) in Southern Spain. *Aquaculture* 217(1):179-190.

Joshi, J. B., V. S. Vitankar, A. A. Kulkarni, M. T. Dhotre, and K. Ekambara. 2002. Coherent flow structures in bubble column reactors. *Chemical Engineering Science* 57(16):3157-3183.

Kagan, J. 2010. Third and fourth generation biofuels: Technologies, markets and economics through 2015. *Boston-NYC-San Francisco: Greentech Media.*

Kaidi, F., R. Rihani, A. Ounnar, L. Benhabyles, and M. W. Naceur. 2012. Photobioreactor design for hydrogen production. *Procedia Engineering* 33:492-498.

Kantarci, N., F. Borak, and K. O. Ulgen. 2005. Bubble column reactors. *Process Biochemistry* 40(7):2263-2283.

Katsuda, T., R. Yegani, N. Fujii, K. Igarashi, S. Yoshimura, and S. Katoh. 2004. Effects of light intensity distribution on growth of Rhodobacter capsulatus. *Biotechnology progress* 20(3):998-1000.

Kemp, L., and S. Lyutse. 2011. Second harvest: bioenergy from cover crop biomass. *Natural Resources Defense Council, March*.

Koc, C., G. A. Anderson, and A. Kommareddy. 2013. Use of red and blue light-emitting diodes (LED) and fluorescent lamps to grow microalgae in a photobioreactor. *Isr J Aquac* 65:797-805.

Kommareddy, A., and G. Anderson. 2003a. Design and construction of light guides for efficient transfer of light in to a dense algal culture in a Photo-Bio Reactor (PBR). In *2003 ASAE Annual Meeting*. American Society of Agricultural and Biological Engineers.

Kommareddy, A., and G. Anderson. 2003b. Study of Light as a parameter in the growth of algae in a Photo-Bio Reactor (PBR). In *2003 ASAE Annual Meeting*. American Society of Agricultural and Biological Engineers.

Kommareddy, R. A., A. A. Gary, P. G. Stephen, and S. B. Ghazi. 2013. The Impact of Air Flow Rate on Photobioreactor Sparger/Diffuser Bubble Size(s) and Distribution.

Krivtsov, V., E. G. Bellinger, and D. C. Sigee. 1999. Modelling of elemental associations in Anabaena. *Hydrobiologia* 414:75-81.

Kulkarni, A. V., and J. B. Joshi. 2011a. Design and selection of sparger for bubble column reactor. Part I: Performance of different spargers. *Chemical Engineering Research and Design* 89(10):1972-1985.

Kulkarni, A. V., and J. B. Joshi. 2011b. Design and selection of sparger for bubble column reactor. Part II: Optimum sparger type and design. *Chemical Engineering Research and Design* 89(10):1986-1995.

Kulkarni, A. V., S. S. Roy, and J. B. Joshi. 2007. Pressure and flow distribution in pipe and ring spargers: Experimental measurements and CFD simulation. *Chemical Engineering Journal* 133(1–3):173-186.

Kumar, K., C. N. Dasgupta, B. Nayak, P. Lindblad, and D. Das. 2011. Development of suitable photobioreactors for CO 2 sequestration addressing global warming using green algae and cyanobacteria. *Bioresource technology* 102(8):4945-4953.

Kunjapur, A. M., and R. B. Eldridge. 2010. Photobioreactor design for commercial biofuel production from microalgae. *Industrial & Engineering Chemistry Research* 49(8):3516-3526.

Lee, C.-G., and B. Ø. Palsson. 1996. Photoacclimation of Chlorella vulgaris to Red Light from Light-Emitting Diodes Leads to Autospore Release Following Each Cellular Division. *Biotechnology progress* 12(2):249-256.

Lee, Y. K., and C. S. Low. 1992. Productivity of outdoor algal cultures in enclosed tubular photobioreactor. *Biotechnology and bioengineering* 40(9):1119-1122.

Low, C., and M. I. Toledo. 2015. Assessment of the shelf-life of Nannochloropsis oculata flocculates stored at different temperatures/Evaluación de la vida útil de floculados de Nannochloropsis oculata almacenados a distintas temperaturas de conservación. *Latin American Journal of Aquatic Research* 43(2):315.

Lü, J., C. Sheahan, and P. Fu. 2011. Metabolic engineering of algae for fourth generation biofuels production. *Energy & Environmental Science* 4(7):2451-2466.

Luff, B. B., and R. B. Reed. 1978. Standard enthalpies of formation of monopotassium and dipotassium orthophosphate. *Journal of Chemical and Engineering Data* 23(1):60-62.

Luque, R., L. Herrero-Davila, J. M. Campelo, J. H. Clark, J. M. Hidalgo, D. Luna, J. M. Marinas, and A. A. Romero. 2008. Biofuels: a technological perspective. *Energy & Environmental Science* 1(5):542-564.

Mahapatra, D. M., H. N. Chanakya, and T. V. Ramachandra. 2013. Euglena sp. as a suitable source of lipids for potential use as biofuel and sustainable wastewater treatment. *Journal of Applied Phycology* 25(3):855-865.

Martin, J. 2010. The billion gallon challenge: Getting biofuels back on track. *Washington, DC: Union of Concerned Scientists*.

Martin, J. 2013. The billion gallon challenge: Getting biofuels back on track. *Washington, DC: Union of Concerned Scientists*.

Mata, T. M., A. A. Martins, and N. S. Caetano. 2010. Microalgae for biodiesel production and other applications: A review. *Renewable and Sustainable Energy Reviews* 14(1):217-232.

Matos, Â. P., R. Feller, E. H. S. Moecke, J. V. de Oliveira, A. F. Junior, R. B. Derner, and E. S. Sant'Anna. 2016. Chemical Characterization of Six Microalgae with Potential Utility for Food Application. *Journal of the American Oil Chemists' Society* 93(7):963-972.

Matthijs, H. C. P., H. Balke, U. M. van Hes, B. M. A. Kroon, L. R. Mur, and R. A. Binot. 1996. Application of light-emitting diodes in bioreactors: Flashing light effects and

energy economy in algal culture (Chlorella pyrenoidosa). *Biotechnology and bioengineering* 50(1):98-107.

Milledge, J., and S. Heaven. 2013. A review of the harvesting of micro-algae for biofuel production. *Reviews in Environmental Science and Bio/Technology* 12(2):165-178.

Miller, D. N. 1980. Gas Holdup and Pressure Drop in Bubble Column Reactors. *Industrial & Engineering Chemistry Process Design and Development* 19(3):371-377.

Miron, A. S., A. C. Gomez, F. G. Camacho, E. M. Grima, and Y. Chisti. 1999. Comparative evaluation of compact photobioreactors for large-scale monoculture of microalgae. *Journal of biotechnology* 70(1):249-270.

Molina, E., J. Fernández, F. G. Acién, and Y. Chisti. 2001. Tubular photobioreactor design for algal cultures. *Journal of biotechnology* 92(2):113-131.

Molina Grima, E., F. García Camacho, S. P. Ja, J. Urda Cardona, and F. S. Jm. 1994. Outdoor chemostat culture of Phaeodactylum tricornutum UTEX 640 in a tubular photobioreactor for the production of eicosapentaenoic acid. *Biotechnology and applied biochemistry* 20(2):279-290.

Morweiser, M., O. Kruse, B. Hankamer, and C. Posten. 2010. Developments and perspectives of photobioreactors for biofuel production. *Applied Microbiology and Biotechnology* 87(4):1291-1301.

Moser, B. K., and G. R. Stevens. 1992. Homogeneity of variance in the two-sample means test. *The American Statistician* 46(1):19-21.

Munoz, R., and B. Guieysse. 2006. Algal–bacterial processes for the treatment of hazardous contaminants: a review. *Water Research* 40(15):2799-2815.

Ogbonna, J. C., and H. Tanaka. 2000. Light requirement and photosynthetic cell cultivation–Development of processes for efficient light utilization in photobioreactors. *Journal of Applied Phycology* 12(3-5):207-218.

Ogbonna, J. C., H. Yada, H. Masui, and H. Tanaka. 1996. A novel internally illuminated stirred tank photobioreactor for large-scale cultivation of photosynthetic cells. *Journal of Fermentation and Bioengineering* 82(1):61-67.

Ogbonna, J. C., H. Yada, and H. Tanaka. 1995. Light supply coefficient: a new engineering parameter for photobioreactor design. *Journal of Fermentation and Bioengineering* 80(4):369-376.

Olguí, E. J. 2003. Phycoremediation: key issues for cost-effective nutrient removal processes. *Biotechnology Advances* 22(1):81-91.

Park, J. B. K., R. J. Craggs, and A. N. Shilton. 2011. Wastewater treatment high rate algal ponds for biofuel production. *Bioresource technology* 102(1):35-42.

Perlack, R. D., L. L. Wright, A. F. Turhollow, R. L. Graham, B. J. Stokes, and D. C. Erbach. 2005. Biomass as feedstock for a bioenergy and bioproducts industry: the technical feasibility of a billion-ton annual supply. Oak Ridge National Lab TN.

Posten, C. 2009. Design principles of photo-bioreactors for cultivation of microalgae. *Engineering in Life Sciences* 9(3):165-177.

Posten, C. 2012. Design and performance parameters of photobioreactors. *Technikfolgenabschätzung–Theorie und Praxis (TATuP)* 21:38-45.

Pozza, C., S. Schmuck, and T. Mietzel. A novel photobioreactor with internal illumination using Plexiglas rods to spread the light and LED as a source of light for wastewater treatment using microalgae.

Pozza, C., S. Schmuck, and T. Mietzel. 2012. A novel photobioreactor with internal illumination using Plexiglas rods to spread the light and LED as a source of light for wastewater treatment using microalgae. *Germany: Department of Urban Water and Waste Management[WWW]* https://keynote. *conferenceservices. net/resources/444/2653/pdf/IWAWCE2012_0189. pdf (2.03. 2015)*.

Pragya, N., K. K. Pandey, and P. K. Sahoo. 2013. A review on harvesting, oil extraction and biofuels production technologies from microalgae. *Renewable and Sustainable Energy Reviews* 24(0):159-171.

Priyadarshani, I., and B. Rath. 2012. Commercial and industrial applications of micro algae–A review. *J algal biomass utln* 3(4):89-100.

Prokop, A., R. K. Bajpai, and M. E. Zappi. 2015. *Algal Biorefineries: Volume 2: Products and Refinery Design*. Springer.

Pruvost, J., J. Legrand, P. Legentilhomme, and A. Muller-Feuga. 2002. Simulation of microalgae growth in limiting light conditions: flow effect. *AIChE Journal* 48(5):1109-1120.

Rajendran, A. 2016. Behavior of Light in a Photobioreactor and Design of Light Guides.

Rawat, I., R. R. Kumar, T. Mutanda, and F. Bux. 2011. Dual role of microalgae: phycoremediation of domestic wastewater and biomass production for sustainable biofuels production. *Applied Energy* 88(10):3411-3424.

Rolfe, M. D., C. J. Rice, S. Lucchini, C. Pin, A. Thompson, A. D. S. Cameron, M. Alston, M. F. Stringer, R. P. Betts, and J. Baranyi. 2012. Lag phase is a distinct growth phase that prepares bacteria for exponential growth and involves transient metal accumulation. *Journal of bacteriology* 194(3):686-701.

Ruffing, A. M. 2011. Engineered cyanobacteria: teaching an old bug new tricks. *Bioengineered bugs* 2(3):136-149.

Ruxton, G. D. 2006. The unequal variance t-test is an underused alternative to Student's t-test and the Mann–Whitney U test. *Behavioral Ecology* 17(4):688-690.

Schneider, D. 2006. Grow Your Own? *American Scientist* 94(5):408-409.

Sharathchandra, K., and M. Rajashekhar. 2011. Total lipid and fatty acid composition in some freshwater cyanobacteria. *J. Algal Biomass Utln* 2(2):83-97.

Shelef, G., A. Sukenik, and M. Green. 1984. Microalgae harvesting and processing: a literature review. Technion Research and Development Foundation Ltd., Haifa (Israel).

Sheppard, C. J. R., X. Gan, M. Gu, and M. Roy. 2006. Signal-to-noise ratio in confocal microscopes. *Handbook of biological confocal microscopy*:442-452.

Shu, C.-H., C.-C. Tsai, W.-H. Liao, K.-Y. Chen, and H.-C. Huang. 2012. Effects of light quality on the accumulation of oil in a mixed culture of Chlorella sp. and Saccharomyces cerevisiae. *Journal of Chemical Technology & Biotechnology* 87(5):601-607.

Sierra, E., F. G. Acién, J. M. Fernández, J. L. García, C. González, and E. Molina. 2008. Characterization of a flat plate photobioreactor for the production of microalgae. *Chemical Engineering Journal* 138(1):136-147.

Silberberg, M. S. 2007. *Principles of general chemistry*. McGraw-Hill Higher Education.

Singh, A., P. S. Nigam, and J. D. Murphy. 2011. Mechanism and challenges in commercialisation of algal biofuels. *Bioresource technology* 102(1):26-34.

Singh, J., and S. Gu. 2010. Commercialization potential of microalgae for biofuels production. *Renewable and Sustainable Energy Reviews* 14(9):2596-2610.

Singh, R. N., and S. Sharma. 2012. Development of suitable photobioreactor for algae production–A review. *Renewable and Sustainable Energy Reviews* 16(4):2347-2353.

Socher, M. L., C. Löser, C. Schott, T. Bley, and J. Steingroewer. 2016. The challenge of scaling up photobioreactors: Modeling and approaches in small scale. *Engineering in Life Sciences* 16(7):598-609.

Soman, A., and Y. Shastri. 2015. Optimization of novel photobioreactor design using computational fluid dynamics. *Applied Energy* 140:246-255.

Stanier, R. Y., R. Kunisawa, M. Mandel, and G. Cohen-Bazire. 1971. Purification and properties of unicellular blue-green algae (order Chroococcales). *Bacteriological reviews* 35(2):171.

Ting, H., L. Haifeng, M. Shanshan, Y. Zhang, L. Zhidan, and D. Na. 2017. Progress in microalgae cultivation photobioreactors and applications in wastewater treatment: A review. *International Journal of Agricultural and Biological Engineering* 10(1):1.

Tranmer, M., and M. Elliot. 2008. Multiple linear regression. *The Cathie Marsh Centre for Census and Survey Research (CCSR)*.

Tredici, M. R., and G. C. Zittelli. 1998. Efficiency of sunlight utilization: tubular versus flat photobioreactors. *Biotechnology and bioengineering* 57(2):187-197.

Uyar, B., I. Eroglu, M. Yücel, U. Gündüz, and L. Türker. 2007. Effect of light intensity, wavelength and illumination protocol on hydrogen production in photobioreactors. *International Journal of Hydrogen Energy* 32(18):4670-4677.

Veera, U. P., and J. B. Joshi. 1999. Measurement of Gas Hold-Up Profiles by Gamma Ray Tomography: Effect of Sparger Design and Height of Dispersion in Bubble Columns. *Chemical Engineering Research and Design* 77(4):303-317.

Verawaty, M., E. Melwita, P. Apsari, and M. Mayumi. 2017. Cultivation Strategy for Freshwater Macro-and Micro-Algae as Biomass Stock for Lipid Production. *Journal of Engineering and Technological Sciences* 49(2):261-274.

Vial, C., S. Poncin, G. Wild, and N. Midoux. 2001. A simple method for regime identification and flow characterisation in bubble columns and airlift reactors. *Chemical Engineering and Processing: Process Intensification* 40(2):135-151.

Vijayakumar, J. 2015. Optimization of Nutrient Requirements, Growth Conditions for Cyanobacteria Using a Flat Plate Reactor and Harvesting by pH Induced Flocculation.

Vree, J. H., R. Bosma, M. Janssen, M. J. Barbosa, and R. H. Wijffels. 2015. Comparison of four outdoor pilot-scale photobioreactors. *Biotechnology for biofuels* 8(1):215.

Wang, B., C. Q. Lan, and M. Horsman. 2012. Closed photobioreactors for production of microalgal biomasses. *Biotechnology Advances* 30(4):904-912.

Xiao, Y., Z. Li, C. Li, Z. Zhang, and J. Guo. 2016. Effect of Small-Scale Turbulence on the Physiology and Morphology of Two Bloom-Forming Cyanobacteria. *PloS one* 11(12):e0168925.

Xu, Z. 2007. Chapter 21 - Biological Production of Hydrogen from Renewable Resources A2 - Yang, Shang-Tian. In *Bioprocessing for Value-Added Products from Renewable Resources*, 527-557. Amsterdam: Elsevier.

Zhan, J., Q. Zhang, M. Qin, and Y. Hong. 2016. Selection and characterization of eight freshwater green algae strains for synchronous water purification and lipid production. *Frontiers of Environmental Science & Engineering* 10(3):548-558.

Zijffers, J.-W. F., M. Janssen, J. Tramper, and R. H. Wijffels. 2008. Design process of an area-efficient photobioreactor. *Marine biotechnology* 10(4):404-415.

APPENDIX

Appendix 1. Atomic weight of elements in biomass

Elements	Atomic mass (g/mol)	No. of mole in composition	Total atomic weight (g)
C	12.0107	44.60	535.677
H	1.0079	7.00	7.055
O	15.9940	25.00	399.850
N	14.0067	7.69	107.571
P	30.9378	0.90	27.844
S	32.0650	0.30	9.620
			1087.617

Nitrogen Calculation

1 mol of biomass =1087.617 g of algae

7.689 mol of $NaNO_3$ = 652.759 g

1087.617 g of biomass requires 652.759 g of $NaNO_3$

1 g of biomass requires 0.600 g of $NaNO_3$

Weight of nitrogen in 7.689 mole $NaNO_3$

= (107.571g/652.173 g) * 100

= 16.48% of $NaNO_3$

Therefore, Nitrogen required for 1 g of biomass = 0.0989 g

Phosphorous Calculation

1 mol of biomass =1087.617 g of algae

0.9 mol of K_2HPO_4 = 156.758 g

1087.617 g of biomass requires 156.758 g of K_2HPO_4

1 g of biomass requires 0.144 g of K_2HPO_4

Weight of Phosphorous in 0.9 mole K_2HPO_4

= (27.844g/156.758 g) * 100

= 17.76 % of K_2HPO_4

Therefore, phosphorous required for 1 g of biomass = 0.026 g

Sulphur Calculation

1 mol of biomass =1087.617 g of algae

0.3 mol of $MgSO_4$ = 36.110 g

1087.617 g of biomass requires 36.110 g of $MgSO_4$

1 g of biomass requires 0.033 g of $MgSO_4$

Weigh of Sulphur in 0.3 mole $MgSO_4$

= (9.620g/36.110 g) * 100

= 26.64 % of $MgSO_4$

Therefore, Sulphur required for 1 g of biomass = 0.009g

Carbon Calculation

Concentration of gas in the available tank

CO_2 =95%, N_2 =5%

Now, properties of CO_2 in the available tank at room temperature:

P=600 psi=40.83atm (after the tank before reaching the flow rate)

M=44g/mol of CO_2

T=298.5K

R=0.0821 L.atm/mol.K

Volume = $0.043m^3$

Therefore, Concentration of Carbon dioxide

m/V =PM/RT

= (40.83atm *44g/mol*0.95) / (0.0821 L. atm/mol. K *298.5K*$0.043m^3$)

=1619.57g CO_2/m^3

1 mol of algae =44.6 mol of CO_2

= 44.6 mol*(12.0107+15.994*2) g/ mol

= 1962.34 g

Now,

1087.62 g algae =1962.34 g of CO_2

1g of algae =1.80 g of CO_2

1000 g of algae =1800 g of CO_2

Therefore,

1 mol of biomass =1087.617g

44.6 mole of CO_2 =1962.34 g

1087.617g of biomass requires 1962.34 g of CO_2

1g of biomass requires 1.804 g of CO_2

Carbon weightage =0.272

=27.29% of CO_2

Therefore, Carbon required for 1 g of biomass =0.492g

Appendix 2. Atomic weight of compounds.

S. N	Compounds	Atomic mass (g/mol)	No. of mole	Total atomic weight (g)
1	$NaNO_3$	84.9946	7.68	652.759
2	K_2HPO_4	174.1759	0.9	156.758
3	$MgSO_4$	120.3676	0.3	36.110

Appendix 3. Energy balance calculation details

From Material balance:

44.6 mole of CO_2 is required to produce 1 mole of $C_{44.6}H_7O_{25}N_{7.68}P_{0.9}S_{0.3}$

1 mole of $C_{44.6}H_7O_{25}N_{7.68}P_{0.9}S_{0.3}$ = 1087.617 g algae biomass

44.6 mole of CO_2 = 1087.617 g algae biomass

Now, roughly 10 photons are required to fix one carbon atom.

$$E = \frac{hc}{\lambda}$$

h =$6.636*10^{-34}$ J.s

λ = 680 nm

C =$2.998*10^{8}$m/s

$$E = \frac{6.636 * 10^{-34}\,\text{J.s} * 2.998 * 10^{8}\ m/s}{680\ \text{nm} *\ 10^{-9} m}$$

$Energy\ of\ a\ photon = 2.9257 * 10^{-19} \quad J/Photon$

Carbon atoms in 1 mole of biomass $=44.6*6.022*10^{23}$

$=2.686*10^{25}$

10 photons / carbon x $2.686*10^{25}$ carbon / mole

$=2.686*10^{26}$ photons per mole of biomass

Energy required to fix carbon atoms in 1 mole of biomass

$= 2.9257*10^{-19}$J/Photons$*2.686*10^{26}$ photons

=78,584,302 J

Energy Breakdown

$44.6CO_2 + 7.6NaNO_3 + 0.9K_2HPO_4 + 0.3MgSO_4 + 6.55H_2O$-- $C_{44.6}H_7O_{25}N_{7.68}P_{0.9}S_{0.3}$ +

$7.68NaOH + 0.3\ Mg\ (OH)_2 + 1.8KOH + 45.025O_2$

Compounds/elements	Standard Enthalpies (KJ/mol)(Luff and Reed, 1978; Silberberg, 2007; Vree et al., 2015)
O_2	0
CO_2	-393.5
H_2O	-241.8
$NaNO_3$	-446.2
K_2HPO_4	-376.1
$MgSO_4$	-1278.2
NaOH	-469.6
$Mg(OH)_2$	-924.7
KOH	-424.76
Biomass	-22.5KJ/g (Vree et al., 2015) = - 22.5/0.000919 KJ/mol (1 mol of biomass=1087.617g) = -24483.134 KJ/mol

Energy calculation for reactants

=44.6*(-393.5) + 7.6*(-446.2) + 0.9*(-376.1) + 0.3*(-1278.2) + 6.55*(-241.8)

= -23246.96 KJ

Energy calculation for products

= 1*(-24483.134) + 7.68 *(-469.6) + 0.3*(-924.7) + 1.8*(-424.76) + 44.25*0

= -27047.684 KJ

Energy Difference

= (-28780.25) – (-27047.684) KJ

= -3800.724 KJ

Appendix 4. Randomized block design test for light intensity analysis (Rajendran, 2016)

Treatment	Flow rate	Depth of Photobioreactor (pathlength)				
	(LPM)	102mm	152mm	203mm	254mm	305mm
		(4")	(6")	(8")	(10")	(12")
	1	83.23	77.18	63.3	53.13	52.38
	2	75.52	72.67	59.63	52.4	48.74
	3	72	70.07	58.01	51.21	47.6
	4	68.44	67.49	57.65	50.14	46.68
	5	67.03	64.46	53.52	49.19	45.81
	6	61.24	62.37	55.13	49.16	40.95
	7	64.13	60.33	53.88	48.73	42
	8	60.1	57.64	50.83	48.87	40.95
	9	60.23	56.02	51.69	48.11	39.28
	10	56.62	54.24	50.34	48.99	39.58
Treatment = Path length Block =Flowrate Number of samples (n)=50				Number of treatment =5 Number of block =10		

.

Appendix 5. Output of Tukey HSD test between the pathlengths

$statistics

MS error	Df	Mean	CV	MSD	
8.749007	47	56.1778		5.265197	3.752108

$parameters

test	name.t	ntr	Studentized Range	alpha
Tukey	Pathlength	5	4.0114	0.05

$means

	Intensity	std	r	Min	Max	Q25	Q50	Q75
102	66.854	8.202076	10	56.62	83.23	60.4825	65.580	71.1100
152	64.247	7.549991	10	54.24	77.18	58.3125	63.415	69.4250
203	55.398	4.194544	10	50.34	63.30	52.1475	54.505	57.9200
254	49.993	1.695871	10	48.11	53.13	48.9000	49.175	50.9425
305	44.397	4.459126	10	39.28	52.38	40.9500	43.905	47.3700

$comparison

NULL

$groups

	Intensity	groups
102	66.854	a
152	64.247	a
203	55.398	b
254	49.993	c
305	44.397	d

Appendix 6. Output of Tukey HSD test for flowrate

$parameters

test	name.t	ntr	Studentized Range	alpha
Tukey	Flowrate	10	4.694934	0.05

$means

	Intensity	std	r	Min	Max	Q25	Q50	Q75
1	65.844	13.965806	5	52.38	83.23	53.13	63.30	77.18
2	61.792	11.937624	5	48.74	75.52	52.40	59.63	72.67
3	59.778	10.956079	5	47.60	72.00	51.21	58.01	70.07
4	58.080	9.862381	5	46.68	68.44	50.14	57.65	67.49
5	56.002	9.348731	5	45.81	67.03	49.19	53.52	64.46
6	53.770	8.905265	5	40.95	62.37	49.16	55.13	61.24
7	53.814	8.864256	5	42.00	64.13	48.73	53.88	60.33
8	51.678	7.585669	5	40.95	60.10	48.87	50.83	57.64
9	51.066	8.008716	5	39.28	60.23	48.11	51.69	56.02
10	49.954	6.547968	5	39.58	56.62	48.99	50.34	54.24

$comparison

NULL

$groups

	Intensity	groups
1	65.844	a
2	61.792	ab
3	59.778	abc
4	58.080	bc
5	56.002	bcd
7	53.814	cd
6	53.770	cd
8	51.678	d
9	51.066	d
10	49.954	d

attr(,"class")

[1] "group"

Appendix 7. Linear regression results for light intensity analysis

```
Call:
lm(formula = Intensity ~ Pathlength+Flowrate+Pathlength*Flowrate)
Residuals:
   Min          1Q          Median          3Q          Max
-5.4728      -1.8931      0.0562          1.3166      5.6291
Coefficients:
                          Estimate    Std. Error      t value      Pr(>|t|)
(Intercept)             98.409426    2.176694       45.210        < 2e-16 ***
Pathlength               -0.162947    0.010099       -16.134        < 2e-16 ***
Flowrate                 -3.373760    0.350806       -9.617          1.39e-12 ***
Pathlength:Flowrate  0.008442   0.001628   5.187 4.69e-06 ***
---
Signif. codes:  0 '***' 0.001 '**' 0.01 '*' 0.05 '.' 0.1 ' ' 1

Residual standard error: 2.375 on 46 degrees of freedom
Multiple R-squared:  0.9486,  Adjusted R-squared:  0.9453
F-statistic:   283 on 3 and 46 DF, p-value: < 2.2e-16
```

Appendix 8. Biomass concentration data and its physical parameters

Days	Biomass (mg/L)	ORP (mV)	DO (mg/l)	pH	Temp (°C)
0	10.00	294.34	8.68	7.51	26.81
1	14.00	327.67	8.60	6.82	28.95
2	91.00	302.52	8.68	6.15	29.83
3	248.00	283.87	8.64	6.31	30.45
4	271.00	274.17	8.64	6.50	30.41
5	299.00	257.38	8.53	6.51	30.32
6	386.00	248.33	8.56	6.49	30.66
7	426.00	255.10	8.47	6.47	30.91
8	404.00	260.44	8.40	6.50	30.13
9	434.00	260.91	8.51	6.72	29.42
10	433.00	256.17	8.50	6.91	29.28
11	451.60	266.25	8.50	6.69	29.25
12	695.00	271.69	8.40	6.38	29.06
13	928.00	257.97	8.24	6.37	29.85
14	686.00	244.14	8.20	7.12	30.03
15	577.00	202.06	8.32	7.43	29.68
16	170.00	169.76	8.47	8.09	29.50

Appendix 9. Regression analysis of biomass on ORP, pH, DO, and temperature

```
Call:
lm(formula = Biomass ~ ORP + pH + DO + Temperature)
Residuals:
   Min        1Q    Median        3Q       Max
-161.428   -25.389     9.741    38.449   104.728
Coefficients:
             Estimate   Std. Error   t value   Pr(>|t|)
(Intercept)  18844.900  1989.858     9.470     6.43e-07 ***
ORP          -3.626      1.170       -3.098    0.009233 **
pH           -1377.045   160.978     -8.554    1.88e-06 ***
DO           -403.263    82.544      -4.885    0.000375 ***
Temperature  -104.323    36.424      -2.864    0.014245 *
---
Signif. codes:  0 '***' 0.001 '**' 0.01 '*' 0.05 '.' 0.1 ' ' 1
Residual standard error: 76.73 on 12 degrees of freedom
Multiple R-squared:  0.9279,  Adjusted R-squared:  0.9039
F-statistic:  38.6 on 4 and 12 DF, p-value: 9.234e-07
```

Appendix 10. Biomass Concentration and flow rate data

Days	Biomass (mg/L)	Air flow rate (l/min)	CO_2 flow rate (ml/min)
0	10.00	14.00	0
1	14.00	14.00	67.63
2	91.00	14.00	124.05
3	248.00	14.00	93.76
4	271.00	14.00	62.03
5	299.00	14.00	62.03
6	386.00	17.00	108.55
7	426.00	20.00	155.07
8	404.00	20.59	155.07
9	434.00	30.00	146.43
10	433.00	30.00	218.5
11	451.60	30.00	310.22
12	695.00	30.00	310.13
13	928.00	30.01	310.19
14	686.00	40.00	217.86
15	577.00	40.00	144.81
16	170.00	40.00	0

Appendix 11. Regression analysis of biomass on CO_2flow and Airflow

Call:
lm(formula = Biomass ~ CO_2flow + Airflow)

Residuals:

Min	1Q	Median	3Q	Max
-253.24	-84.09	29.60	77.58	223.14

Coefficients:

	Estimate	Std. Error	t value	Pr(>|t|)
(Intercept)	-45.1954	88.6100	-0.510	0.617963
CO_2flow	1.6942	0.3759	4.507	0.000492 ***
Airflow	7.4821	3.7185	2.012	0.063856.

Signif. codes: 0 '***' 0.001 '**' 0.01 '*' 0.05 '.' 0.1 ' ' 1

Residual standard error: 134.7 on 14 degrees of freedom
Multiple R-squared: 0.7409, Adjusted R-squared: 0.7038
F-statistic: 20.01 on 2 and 14 DF, p-value: 7.847e-05